



# **Manual of kSEMAWc 2.3 software**

**Marco Montecchi**

ENEA – C.R. Casaccia, Via Anguillarese 301, 00123 – Rome, Italy  
e-mail: marco.montecchi@enea.it



# Contents

<b>1</b>	<b>What kSEMAWc can do</b>	<b>3</b>
<b>2</b>	<b>Computer notes</b>	<b>7</b>
2.1	Source file compilation in Linux operative systems . . . . .	7
2.2	Source file compilation in Windows operative systems . . . . .	8
2.3	Windows executable installation . . . . .	10
2.4	General notes . . . . .	10
<b>3</b>	<b>How to use kSEMAWc</b>	<b>11</b>
3.1	Valin TAB . . . . .	13
3.2	Model TAB . . . . .	19
3.3	Simulation TAB . . . . .	22
3.4	TAB Numerical Search . . . . .	26
3.5	Data Fit TAB . . . . .	30
3.6	Graph range TAB . . . . .	33
<b>4</b>	<b>Mini-guide to the characterization procedure</b>	<b>34</b>
<b>A</b>	<b>Oscillators expressions</b>	<b>37</b>
A.1	Lorentz oscillator . . . . .	39
A.2	Homogeneous quantum oscillator . . . . .	39
A.3	Lorentz-Dirac oscillator . . . . .	40
A.4	Inhomogeneous quantum oscillator . . . . .	41
A.5	Flat oscillator . . . . .	41
A.6	Drude oscillator . . . . .	42
A.7	Drude-ionized oscillator . . . . .	43
A.8	Direct and Indirect gap oscillators . . . . .	44
A.9	Oscillators with an Urbach tail at the band edges . . . . .	51
A.10	Direct Gap Tauc-Exciton oscillator . . . . .	52
A.11	3D M1-M2 critical points oscillator . . . . .	53
<b>B</b>	<b>Some useful rules of good practice</b>	<b>56</b>
B.1	$n, k$ of the substrate . . . . .	56
B.2	Reflectance reference . . . . .	56
B.3	Prismatic sample . . . . .	57
B.4	Masks for small area samples . . . . .	57
B.5	Irregular thickness of the thin film . . . . .	57
B.6	Scan speed and integration time . . . . .	58
B.7	Jump at the grating-detector change . . . . .	58
B.8	Misaligned spectrophotometer . . . . .	58

Many thanks to:

- Alberto Mittiga for his factual collaboration in improving optical constant models about electronic transitions in materials with continuous state density, in the Windows porting as well as the drafting of the manual
- Enrico Nichelatti for the wise search for analytical solutions of the integrals on the density of the states, as well as for the transfer in L<sup>A</sup>T<sub>E</sub>X of this manual
- Claudia Malerba and Francesca Menchini for their constant goad to test and improve kSEMAWc to characterize semiconductor materials
- Francesco Biccari for his useful suggestions for simplifying the software distribution
- Luca Serenelli for his support in outlining the Linux installation procedure
- Giacomo Mazzamuto for his support in the compilation and linking of the GSL library under Windows

# 1 What kSEMAWc can do

kSEMAWc (Spectro-Ellipsometric Measurement Analysis Workbench) is a workspace for the analysis of Spectrophotometric (SP), Ellipsometric (ELI) and Photothermal Deflection Spectroscopy (PDS) measurements. The letter “k” indicates the use of the Qt libraries to generate the graphical user interface, typical of the desktop Linux KDE environment. The last letter “c” indicates the full software rewriting in C++; considering this major improvement, the name was changed to kSEMAWc since the version 1.0.0.

kSEMAWc allows to:

1. simulate SP, ELI and PDS measurements of a multilayer structure, knowing the thicknesses and the complex refractive indexes  $\tilde{n} = n - ik$  of each material composing the different layers<sup>1</sup>;
2. calculate the complex refractive index  $n - ik$  and the thickness of a given “thin” layer from experimental measurements (SP, ELI, PDS), knowing the thicknesses and the complex refractive indexes of all the other layers composing the structure;
3. optimize the parameters of the multilayer model by best-fitting of experimental measurements;
4. evaluate the mean value of physical quantities (for example transmittance or reflectance), weighted on a given international standard spectrum (such as the illuminant D65 or the direct solar spectrum ASTM G173-03) or on a customized reference spectrum (for example the crystal scintillator PbWO<sub>4</sub> luminescence spectrum, used in the CMS experiment at CERN LHC);
5. predict reflectance/transmittance angular trends, once the realistic model of the coating has been set or by means of the equivalent model algorithm [1]; where necessary output spectra can be weighted over a given reference spectrum.

From kSEMAW 0.8.0 onwards, the calculation of the near-specular solar-reflectance as a function of the acceptance angle (mirrors for Concentrated Solar Power) has been removed, because the new software SMQexpo, specific for solar mirrors, equipped with a more advanced equivalent model, is now available. Such software embraces the Open Source philosophy and is freely downloadable from  
<https://github.com/mmonty1960/EMA4SM>.

kSEMAWc uses a mathematical approach based on transfer matrices, particularly suitable for the case of multilayers: in addition to being able to treat coherent propagation and interference (for arbitrary incidence angles), it also allows to simulate the effects due to different types of non-ideal material features, such as optical constants gradients along the film thickness, thickness inhomogeneity, porosity and roughness. The latter is modelled by assuming the thickness to be Gaussian-like distributed with standard deviation  $\sigma$ , and variations along distances much greater than the wavelength  $\lambda$ . The program deals with moderately rough interfaces ( $\sigma \ll \lambda$ ) and limited radiation diffusion [2].

kSEMAWc can model devices composed by up to 9 layers of different materials. For each layer it is possible to: i) consider it as optically *thin* or *thick* with respect to the

---

<sup>1</sup>kSEMAWc adopts the convention of negative sign for the imaginary part of both the complex refractive index and dielectric constant; this convention derives from considering the plane wave solution of the Maxwell equations with positive time expressed as  $\exp[i(\omega t - \mathbf{q} \cdot \mathbf{r})]$ .

radiation coherence length<sup>2</sup>, for summing up coherently or not the contributes originating from its two interfaces in wave propagation; ii) set a refractive index profile along the thickness; iii) introduce roughness at the outermost interface; iv) consider the layer as composed of a mixture of two different materials with optical constants calculated on the basis of the Effective Medium Approximation method. The latter feature can be used to model porosity, by considering the layer as composed by a mixture of material and voids (air) in a given percentage.

To evaluate the unknown  $n$  and  $k$  values of a film starting from experimental measurements the kSEMAWc offers three different methods:

- **Numerical search method;**
- **Standard Fit method;**
- **Hybrid computational method, called “IbridOne”.**

## Numerical search method

Once thickness, and eventually further parameters (roughness, ...), of the unknown layer are set, kSEMAWc can numerically search for the  $(n, k)$  couples of values that reproduce the experimental measurements at any given  $\lambda$ ; the search is exhaustive in the  $n$ -range set by the user.

In the case of a thin film, one or more solutions can exist for each wavelength; in addition, the set of solutions is not necessarily connected. By optimizing the model parameters (thicknesses, roughness, gradients, etc.) according to specific guiding criteria [3,4] detailed in the chapter devoted to this method, a more connected set of solutions can be obtained; finally, among them, a physically reasonable subset of solutions can be selected and saved.

## Standard Fit method

In this method  $n(\lambda)$  and  $k(\lambda)$  are modeled by summing some analytical functions chosen by the user among 13 types of “oscillators”. These functions (described in detail in Appendix A) describe the  $(n, k)$  behavior for a single oscillator centered at a certain resonance energy or for some continuous distributions of oscillators chosen to model the most common distributions for semiconductor materials. These last “oscillators” contain therefore some parameters as the semiconductor band gap and the width and intensity of the absorption band.

When enabled for the best-fit, the oscillators parameters can be optimized by minimizing the merit function

$$MF = \sum_{i,j} [M_{j,cal}(n(\lambda_i), k(\lambda_i)) - M_{j,exp}(\lambda_i)]^2 / \Delta M_{j,exp}(\lambda_i) \quad (1)$$

with the Levenberg Marquardt non-linear least squares curve fitting (offered by the C/C++ MINPACK library prepared by Frédéric Devernay). If the fit is run on experimental spectra, also the parameters of the coating model (e.g. thickness, roughness, ...) can be optimized.

---

<sup>2</sup>According to the Heisenberg uncertainty principle the coherence length is  $\Delta l \sim \frac{1}{2\pi} \frac{\lambda^2}{\Delta\lambda}$  where  $\Delta\lambda$  is the radiation band-width.

The  $n(\lambda)$ ,  $k(\lambda)$  curves found using this method are always continuous and satisfy the Kramers-Kronig equation; the fit quality depends on the suitability of the chosen oscillators as well as on the optical model.

## IbridOne computational method

In the IbridOne method:

1.  $n(\lambda)$  is modelled with a set of oscillators as in the previous method;
2. the extinction coefficient  $k_\lambda$  is numerically computed from  $T(\lambda)$  at each sampling  $\lambda$  with the above assumed  $n(\lambda)$ ;
3. the computed reflectance spectrum  $R_{comp}(\lambda)$  or  $\psi_{comp}(\lambda)$  is compared with the experimental one by means of the merit function of Eq. 1;
4. some parameters, enabled by the user, of the assumed  $n(\lambda)$  analytical function as well as of the optical model are optimized by the Levenberg Marquardt non-linear least square algorithm.

Before starting the optimization with the IbridOne method, the function parameters have to be set to initial values good enough to reasonably model  $n(\lambda)$ .

Note that when using IbridOne the transmittance spectrum is always perfectly reproduced by construction.

The IbridOne method was introduced to directly obtain  $k_\lambda$  from the experimental data without the need of a detailed model of all the physical mechanisms (excitons, defects, band tails etc) which can be involved in its behavior and which can produce a very articulated spectrum.

With respect to the Standard Fit method, where both  $n(\lambda)$  and  $k(\lambda)$  have to be modeled and simultaneously used for the fit, IbridOne requires less assumptions since  $k_\lambda$  is numerically-computed from experimental data  $\lambda$  by  $\lambda$ . As matter of fact,  $n(\lambda)$  shows a more regular behavior and therefore its modeling is less critical.

**As general rule, in order to choose the most appropriate analytical functions to be used in Standard Fit or in IbridOne, at least in the initial phase, it is advisable to use the Numerical search method first, to identify the wavelength-behaviour of a physically meaningful solution subset. Otherwise, the choice of oscillator functions should be driven by the physical properties of the material under investigation: in this case the oscillator parameters in the *Simulation* TAB has to be manually adjusted to obtain a first rough reproduction of the experimental curve before launching Standard Fit or IbridOne.**

**In any case, users should never forget that the reliability of the obtained  $n,k$  solutions strictly depends on the correctness of the experimental measurements used as input data. Appendix B reports some rules of good practice to avoid the most common coarse errors causing artefacts in spectrophotometric measurements.**



## 2 Computer notes

kSEMAWc is written in C++ and is provided of a graphical user interface (GUI) for data input-output based on the Qt libraries, which are cross-platforms.

kSEMAWc generates 2D plots based on the Qwt library which is a graphics extension to the Qt GUI application framework.

Code source files, compiled Windows version, user manual as well as a sample of working directories populated with assorted files can be freely downloaded from

<https://github.com/mmonty1960/ksemawc>

kSEMAWc can be installed in different ways: copying the 64bit Windows10 executable version folder or compiling the source files in Linux or Windows OS.

### 2.1 Source file compilation in Linux operative systems

The installation from source files here described requires a basic knowledge of Linux operative systems.

After the installation of his own favourite Linux distro, the user has to install Qt, Qwt, GSL and C/C++ Minpack libraries.

In the following the details of the installation in one of the Linux distros based on Ubuntu are given.

Once Linux runs, the installation steps are:

- a. first of all, before installing new packages, one should update the whole system by typing in a terminal the commands

```
sudo apt-get update  
sudo apt-get dist-upgrade
```

(in the case of error, `sudo dpkg --configure -a` followed by `sudo apt-get install -f`, and then `dist-upgrade`) and finally re-boot. Alternatively one can directly use the update manager by clicking on the small shield icon on the right of the bottom panel.

- b. with the refreshed system, installation of the compilers gcc and g++

```
sudo apt-get install gcc g++
```

- c. library installation

```
sudo apt-get install libcminpack-dev  
sudo apt-get install libgsl-dev
```

- d. qt installation

```
sudo apt-get install qt5-default  
sudo apt-get install qtcreator libqwt-qt5-dev libqwt-headers
```

From this point on, the kSEMAWc installation starts.

1. download the zipped file from <https://github.com/mmonty1960/ksemawc> and extract the folder `Workspace` in the own home folder, for example `/home/user`

2. open a terminal and move to the directory  
`/home/user/Workspace/qtSource/kSEMAWc`  
by typing the command

```
cd /home/user/Workspace/qtSource/kSEMAWc
```

3. compile the project `kSEMAWc.pro` with the command

```
qmake
```

4. complete with the command

```
make
```

and goto item 6.

Alternatively, if one wants to study the C++ sources, launch QtCreator by the application menu (generally, similarly to Windows desktop, there is a button on the left of the bottom panel) and open the file `kSEMAWc.pro` in the folder `Workspace/qtSource/kSEMAWc`. Then agree to the request “configure project” and set all the paths to

```
"/home/user/Workspace/qtSource/kSEMAWc"
```

5. compile by clicking the play button (green triangle) on the bottom-left; when completed, the GUI software will pop-up.
6. create an icon desktop launcher: right-click on the desktop, create launcher, name it `kSEMAWc`, and set command as

```
/home/user/Workspace/qtSource/kSEMAWc/kSEMAWc
```

set the option “open in a terminal” in order to pop-up a terminal window at the launch of the software. Finally set the working directory as `/home/$USER/Workspace`. The icon can be set to your liking

7. launch the software by clicking on the above-created icon-launcher; if required enable “make executable”

## 2.2 Source file compilation in Windows operative systems

The following instructions refer to the installation of all the necessary tools and libraries on Windows10 systems.

The first step is the installation of the Qt and Qwt libraries.

To install Qt the user must first create a Qt account on <https://login.qt.io/login> and then download the online qt installer from the window ”download for open source users” (GPL/LGPL license). The installer is a large file and it will show to the user many different versions. The kSEMAWc executable file distributed at the moment was compiled using the Qt version 5.15.2 and the compiler mingw810\_64 (select this compiler in the folder ”Developer and designer Tools”). Please take also into account that the installation is a long procedure and the user must wait patiently even if nothing seems to proceed.

Once Qt is installed, the user must download the file qwt-6.2.0.zip with the Qwt sources and the html documentation for Windows from  
<https://sourceforge.net/projects/qwt/files/qwt>.

To install Qwt the user has to follow the instruction contained in the "Qwt User's Guide: Installing Qwt" (<https://qwt.sourceforge.io/qwtinstall.html>).

The first step is to unzip the files in the folder C:\Qwt-6.2.0. Then open the terminal Qt 5.12.2 (MinGW8.1.0 64-bit) in the Qt folder of the start bar and type the commands

```
> Cd c:\Qwt-6.2.0
> Qmake qwt.pro
> mingw32-make
```

The next step is to install the library cminpack which contains the minimization routines. To create this library the user has to install Cmake downloading the Windows x64 installer from <https://cmake.org/download/> .

The Cmake directories C:\Program Files\CMakel\bin and C:\Program Files\Tools\mingw810\_64\bin must be inserted in the path environment variables.

Then the user has to download the file cminpack-1.3.8.tar.gz from <http://devernay.free.fr/hacks/cminpack/> and extract the folder in C:\Program Files\Tools\mingw810\_64 .

After that, to create the dll libraries, start a prompt with the administrator privileges and type the following commands:

```
> cd C:\Program Files\Tools\mingw810_64\cminpack-1.3.8:
> mkdir build
> cd build
> cmake .. -G"MinGW Makefiles" -DBUILD_SHARED_LIBS:BOOL=ON
                                         -DCMINPACK_PRECISION=d
> mingw32-make
```

This will create the double precision version dll and dll.a libraries in the build directory.

The following step is to download the kSEMAWc zipped file from <https://github.com/mmonty1960/ksemawc>. This file contains a 64 bit precompiled version of the GLS GNU library for Windows in the folder gsl-2.7 which has to be extracted and copied to the c: directory.

From this point on, the kSEMAWc installation starts:

- extract the folder **Workspace** to any position on the user hard disk
- open the project **Workspace\qtSource\kSEMAWc\ksemawc.pro** from the Qt creator IDE
- in the "Configure Project" window select the "Desktop Qt 5.15.2 MinGW 64-bit" kit
- in "Details" select the folder **Workspace\qtSource\kSEMAWc** for all the three versions (Debug, Release, Profile)
- compile

- create a shortcut to the exe file contained in `Workspace\qtSource\kSEMAWc\bin`

The distributed `bin` directory already contains all the runtime dll required to run `kSEMAWc.exe` as a standalone portable application. These dll were generated following the procedure outlined in <https://doc.qt.io/qt-5/windows-deployment.html>. In short one has to open the terminal Qt 5.12.2 (MinGW8.1.0 64-bit), move to the directory containing `kSEMAWc.exe` and type the command

```
> winddeployqt kSEMAWc.exe
```

This command will insert all the Qt related dll in that directory. The application may require additional 3rd-party libraries which are not taken into account by `winddeployqt`. Their absence will give error messages which contain the name of the required additional dll which has to be retrieved and copied in the same directory as well.

## 2.3 Windows executable installation

The installation of the precompiled Windows executable simply consists in:

- download the zipped file from <https://github.com/mmonty1960/ksemawc>
- extract the folder `Workspace` to any position on the user hard disk
- create a shortcut to the `ksemawc.exe` file contained in `Workspace\qtSource\kSEMAWc\bin`

## 2.4 General notes

1. Please note that new experimental spectra, *nk*-files and project files must be saved in `Workspace` folder.
2. The directory `Workspace` can be renamed as the user prefers.
3. At the first launch, the user should load one of the `.Spj` project files provided with the distribution zip-file, in order to verify the software correct working; as an example by selecting `ito_ve001.1.Spj` several fields in the *Valin* TAB will be automatically filled; surfing to the *Model* TAB, one will observe that the optical model consists of two layer, an inhomogeneous film 2515 Å thick on a 1 mm thick substrate. Surfing to *Simulation* TAB and click the button “Plot Exp. Measures!” four windows  $\lambda-Tn$ ,  $\lambda-Rn$ ,  $\lambda-n$  and  $\lambda-k$  will pop-up: the first two show the transmittance and reflectance spectra; the other two the plots of  $n_\lambda$  e  $k_\lambda$  solutions stored in the file `ito_ve001.4.nk`.

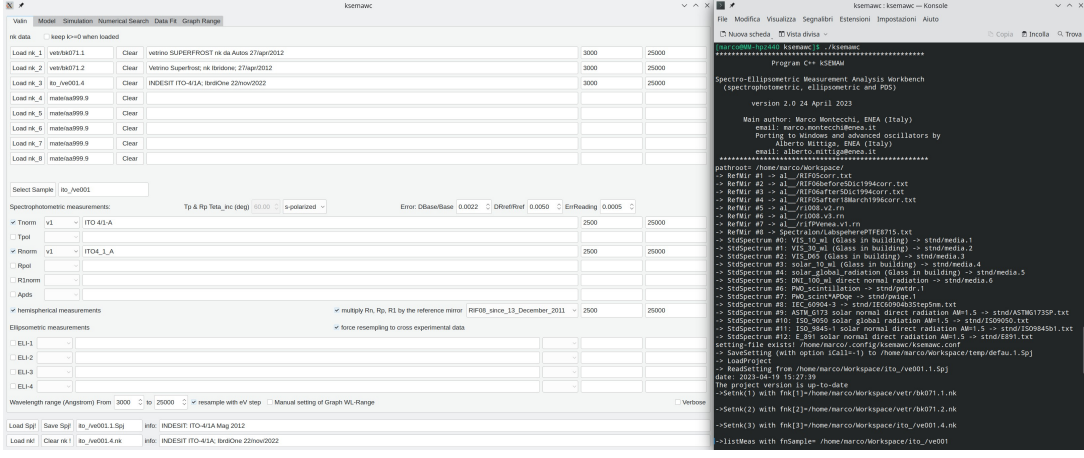


Figure 1: Graphical interface and terminal of kSEMAWc.

### 3 How to use kSEMAWc

Two windows pop-up when kSEMAWc starts: the GUI and a terminal; the latter shows the progress of the workflow in the C++ (kSEMAWc) executable.

The GUI is composed by a top part, structured in 6 “tabs”, ordered in logical sequence, and a bottom part, which is always visible.

The 6 TABs are:

1. **Valin:** selection of  $nk$ -files and measurements to be imported in the analysis work bench.
2. **Model:** setting of the optical device model.
3. **Simulation:** simulation of experimental data on the basis of already known  $nk$ -files and layer model. If an unknown layer is included in the structure, the simulation can be accomplished by setting an oscillators model for its  $n(\lambda)$  and  $k(\lambda)$ ; these curves will be plotted.
4. **Numerical Search:**  $(n_\lambda, k_\lambda)$  of the unknown layer are numerically calculated from a suitable set of measurements as  $T & R, \Delta & \Psi$ , etc.
5. **Data Fit:**  $(n_\lambda, k_\lambda)$  of the unknown layer are obtained by fitting a suitable set of measurements with an oscillator model or by the IbridOne procedure.
6. **Graph Range:** management of plots.

The bottom part, always visible, contains

- loading/saving the SEMAW project file (.Spj)
- loading a  $nk$ -file which data will be displayed in the graphs  $\lambda - n$  and  $\lambda - k$  just for reference.

**Generally speaking, commands in the GUI are written in bold and followed by an exclamation mark.**

File typology	nameBase extensions
Project	.N.Spj
Transmittance at normal incidence	.tN.tn
Transmittance with polarized light	.tN.tp
Reflectance at normal incidence	.tN.rn
Reflectance with polarized light	.tN.rp
Reflectance measured on the back side	.tN.r1
PDS absorptance	.tN.an
Ellipsometric measurement	.N.el
<i>n-k</i>	.N.nk

Table I: Extensions of `nameBase`. Here  $N=0, 1, 2, \dots, 9$ ;  $t="v"$  if in UV-VIS-NIR range, otherwise  $t="i"$  for IR range

**Except *Graph Range* where fonts, window size and line thickness can be set at first, before surfing to another TAB from *Valin*, user must name and save the current project .Spj!**

**Some field/functions are enabled/disabled according to their relevance in the chosen configuration.**

Another important point the user should understand is the adopted philosophy for naming files and folders: kSEMAWc is a software to perform the optical characterization of specimens on the basis of experimental measurements. With time the user will have to manage a multitude of files: some will concern experimental measurements, maybe achieved at different times/conditions; others will represent simulated measurements; others more will be files containing  $n_\lambda, k_\lambda$  data; finally there is the project file, which is the supporting column of the software.

All those files are in the Workspace folder (with the path `/home/$USER/Workspace` in Linux OS), organized in specific subdirectories for each given material/device. All the measurement files related to a single specimen has to be uniquely identified by a `nameBase` adding suitable extensions shown in Table I, where  $N=0, 1, 2, \dots, 9$ ;  $t="v"$  if in UV-VIS-NIR range, otherwise  $t="i"$  for IR range.

Please note that the “near normal incidence” condition applies when the incidence angle is not greater than  $10^\circ$ : as a matter of fact in that angular range measurements do not depend from incidence angle or light-polarization, i.e. the difference is lower than the experimental measurement error.

A short description of each TAB is contained in the following paragraphs.

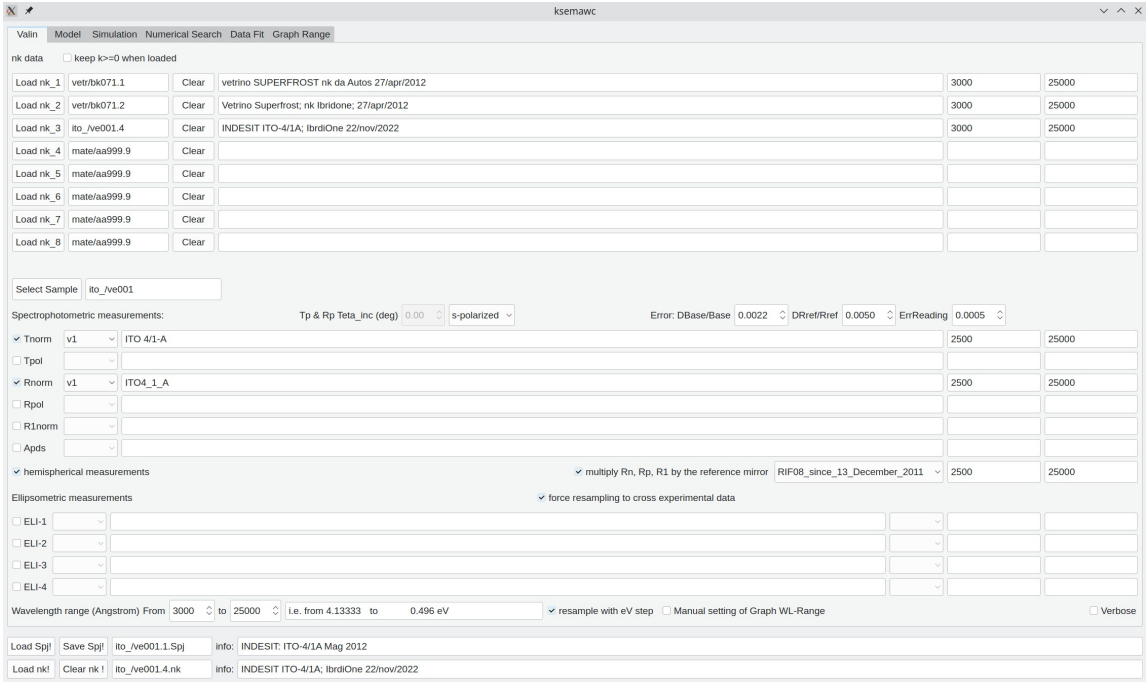


Figure 2: *Valin* TAB.

### 3.1 Valin TAB

When kSEMAWc starts, by default the GUI shows the *Valin* TAB; here *nk*-files and experimental measurements can be set (see Fig. 2).

The block “**nk data**” allows one to set up to 8 *nk*-files containing the complex refractive index of the substrate, of any other layer composing the sample, literature data for the investigated material, and so on.

When the checkbox “keep  $k \geq 0$  when loaded” is ticked, the *nk*-file data are resampled by forcing to 0 any negative  $k$  value; otherwise when negative values are found, a warning pop-up message invites the user to activate that option.

The *nk*-file must be arranged according to the following format:

```
INDESIT ITO-4/1A Ibridone 2/mag/2012
201
3000.0000 1.7586253 0.16867028      2.32177973E-03 9.28342342E-04
3013.2583 1.7548164 0.16510771      2.28923559E-03 7.98091292E-04
...
24115.756 1.3432308 5.45175299E-02 2.32040882E-03 6.11269847E-04
25000.000 1.3170766 6.40117005E-02 2.61688232E-03 6.28869981E-04
```

More precisely, the first row is dedicated to a short info about the file; the second one contains the number of the following records, each one composed by the values  $\lambda(\text{\AA})$ ,  $n$ ,  $k$ ,  $\text{ERR}_n$ ,  $\text{ERR}_k$ , separated by one space or tab; here  $\text{ERR}_n$  and  $\text{ERR}_k$  are the absolute errors on  $n$  and  $k$ , respectively. Data must be ordered with decreasing/increasing wavelength; the wavelength step is not required to be constant. The maximum number of loadable records is 999.

**Angstrom ( $\text{\AA}$ ) is the adopted unit for wavelength in .nk files and for (*thin*) film thickness (millimetre for the (*thick*) bulk ones); conversely the nanometre (nm) is used in the experimental files SP, ELI e PDS!**

In the GUI the row for *nk*-file selection is composed by a first field where `name_file` is displayed; the second field shows the file info; the following other two fields show  $\lambda_{min}$  and  $\lambda_{max}$  of the data wavelength range; all these fields are just informative and cannot be edited.

The experimental measurements can be set in the block “**Spectrophotometric measurements**”. A dialog window for file selection will pop-up when “Select Sample” is pressed; it is sufficient to select just one of the files concerning the specimen of interest marked by `nameBase`, and automatically the software will locate all the available SP, ELI and PDS measurements and, in the case of multiple choice, all the options will be offered in the combo box menu.

Concerning the format of the SP files, all those generated by Perkin-Elmer UV-VIS-NIR and IR instruments, since 1988, are accepted.

Otherwise data should be arranged as in the following example:

```
KN929aCW_csl 10000A Tdiretta
#####SCALED%
2500.
250.
1126
2500 78.090897
2498 80.310163
.....
252 0.003400
250 0.000785
```

where the measured values are in %. In the case of absolute value, i.e. 0.78090897 instead of 78.090897, the second row has to be modified in #####SCALED%.

In any case the meaning of the first rows is:

1. info
2. value type (% or Absolute)
3. initial  $\lambda$
4. final  $\lambda$
5. number of data ( $N$ ).

$N$  rows consisting of the couple of values  $\lambda$  val-measured follow in decreasing/increasing order of  $\lambda$ ; once again the  $\lambda$  step can be not constant.

code-string	Ellipsometric data					
tldp	$\theta$	$\lambda$	$\Delta$	$\Psi$	Err $\Delta$	Err $\Psi$
etpd	$E$	$\theta$	$\Psi$	$\Delta$	Err $\Psi$	Err $\Delta$
ltpd	$\lambda$	$\theta$	$\Psi$	$\Delta$	Err $\Psi$	Err $\Delta$
etcab	$E$	$\tan(\Psi)$	$\cos(\Delta)$	$\alpha$	$\beta$	

Table II: Available formats for the ellipsometric data-files and their respective code-string to use. Energy values are in eV, and angles in degrees.

The format for ellipsometric data is:

#### Comment-line

*M N code-string*

$\theta_1 \ N_1 \ \lambda_{min_1} \ \lambda_{max_1}$

$\theta_2 \ N_2 \ \lambda_{min_2} \ \lambda_{max_2}$

... ... ...

$\theta_M \ N_M \ \lambda_{min_M} \ \lambda_{max_M}$

ellipsometric data as specified by code-string

where the first line is the comment,  $M$  is number of different incidence-angles  $\theta_1, \theta_2, \dots, \theta_M$ ,  $N$  is the total number of experimental data, code string specifies the data format among those listed in Tab. II; then  $M$  rows follow, each one composed by  $\theta_j, N_j, \lambda_{min_j}, \lambda_{max_j}$  with  $j = 1, \dots, M$ ; finally  $N$  rows containing ellipsometric data formatted as declared with code-string. The only constrain on the data order is that for each  $\theta$  the wavelength values are increasing, while the data relative to a given  $\theta$  value can be arbitrarily distributed. As an example:

```
SUB ZNSE ELICAM 5 mm 19.3.92
2 72 tldp
75.00 36 500.0 850.0
60.00 36 500.0 850.0
75.00 500.0 17.583 10.387 0.136 0.060
60.00 500.0 168.283 15.016 0.150 0.036
75.00 510.0 15.948 10.584 0.129 0.060
60.00 510.0 168.840 14.686 0.142 0.035
... ...
75.00 850.0 6.983 12.720 0.299 0.139
60.00 850.0 172.327 12.309 0.952 0.160
```

or

```
SUB ZNSE ELICAM 5 mm 19.3.92
2 72 tldp
60.00 36 500.0 850.0
75.00 36 500.0 850.0
75.00 500.0 17.583 10.387 0.136 0.060
75.00 510.0 15.948 10.584 0.129 0.060
...
75.00 850.0 6.983 12.720 0.299 0.139
```

```

60.00 500.0 168.283 15.016 0.150 0.036
60.00 510.0 168.840 14.686 0.142 0.035
...
60.00 850.0 172.327 12.309 0.952 0.160

```

Once again, the wavelength unit is nanometer. Up-to 4 ellipsometric files can be set.

**To be loaded into the program, please tick the checkbox of the wished measurement.**

The *Valin* TAB offers the possibility to set the parameters used for computing the error of the SP experimental measurements according to the following equations (under the hypothesis of maximum correlation).

For transmittance:

$$\begin{aligned}
T &= \frac{M}{B} \\
\Delta T &= T \left( \frac{\Delta M}{M} + \frac{\Delta B}{B} \right) \\
B &= 1 \rightarrow M = T \\
\implies \Delta T &= T \Delta B + \Delta M
\end{aligned}$$

For reflectance:

$$\begin{aligned}
R &= \frac{M}{B} R_{\text{ref}} \\
\Delta R &= R \left( \frac{\Delta M}{M} + \frac{\Delta B}{B} + \frac{\Delta R_{\text{ref}}}{R_{\text{ref}}} \right) \\
B &= 1 \text{ if } R_{\text{ref}} \approx 1 \\
&\rightarrow M \approx R \\
\implies \Delta R &= R (\Delta B + \Delta R_{\text{ref}}) + \Delta M
\end{aligned}$$

where  $M$  is the measurement,  $B$  is the baseline,  $\Delta B$  is the baseline error,  $\Delta R_{\text{ref}}$  the reflectance relative error of the reference mirror,  $\Delta M$  the reading error of the spectrophotometer; by default the three fields “Error: DBase/Base”, “DRref/Rref” and “ErReading” are set to the typical values: 0.002, 0.005 e 0.0005. As will be discussed later, the measurement errors are used in kSEMAWc for evaluating the uncertainty area of the solution  $n_\lambda, k_\lambda$  and then the errors on  $n$  and  $k$ .

Moreover the software offers the possibility to multiply the experimental reflectance spectra for the reference mirror reflectance, as soon as the file is loaded and re-sampled. To that purpose the user must tick the “multiply Rn Rp R1 by the reference mirror” checkbox and then select the reference mirror in the drop down menu (enabled just after the above ticking).

The drop down menu with the list of the available reference mirrors can be customized by editing the file `referenceMirrors.txt`, located in the folder `kSEMAWc`; the file is composed as follows:

```

RIF05
al__/_RIF05corr.txt
RIF06_before_5_December_1994

```

```

al__/_RIF06before5Dic1994corr.txt
RIF06_after_5_Decembre_1994
al__/_RIF06after5Dic1994corr.txt
RIF05_after_18_March_1996
al__/_RIF05after18March1996corr.txt
RIF08_since_13_December_2011
al__/_ri008.v2.rn
RIF08_after_17_January_2018
al__/_ri008.v3.rn
RIF_PV_ENEA
al__/_rifPVenea.v1.rn

```

Each reference mirror is described by a couple of rows: the first is the name to add in the combo box menu, the second is the path, including the filename, in **Workspace**. In such a way the user can easily suppress undesired items and add those of his interest.

In the case of roughness, kSEMAWc adopts the simplified approach proposed by [2] for evaluating hemispherical<sup>3</sup> or specular (direct) reflectance (transmittance), depending on the checkbox “hemispherical measurements” (ticked or not). Please note that the choice simultaneously holds for transmittance and reflectance.

If some measurements obtained at oblique incidence is selected, the user must set the incidence angle and the polarization type (*s-polarized* or *p-polarized*); the not polarized case is not considered here because it is not useful for optical characterization purposes. Later, the incidence angle can be modified in the *Simulation TAB*.

As soon as *nk*-file and measurements are set, kSEMAWc computes the maximum common wavelength range where data from all the selected inputs are available; the limit values of that range are shown in the field “Wavelength Range (Angstrom)”; the corresponding range in eV is also displayed. By default, that is the range used for resampling both *nk*-file and experimental measurements on a common base of 201 points<sup>4</sup>, with step in wavelength (Å) or in energy (eV) when the checkbox “resample with eV step” is ticked. The latter choice is recommended for thin film coatings because it allows to view the interference fringes with an almost regular period. Higher resolution along a narrower region can be obtained by properly adjusting the two spin boxes just below the label “Wavelength Range (Angstrom)”.

By default the range of the abscissa  $\lambda$  in the drawn plots is set to the maximum common wavelength range; otherwise by ticking “Manual setting of Graph WL-Range” the user can set a different range, both narrower or wider, according to the scale set at the wavelength (“wl”) row of the *Graph Range TAB*.

By default, ellipsometric spectra are resampled constraining the new curve to cross each one of the original experimental data; in the case of noisy spectra, smoother (resampled) spectra can be obtained by unticking the option “force resampling to cross experimental data”.

**Before surfing from *Valin* to another TAB, the user must name and save**

---

<sup>3</sup>reflectance/transmittance obtained by placing the specimen on the suitable port of an integrating sphere is called *hemispherical*; the purpose of that arrangement is to collect the whole radiation transmitted/reflected in the half-space.

<sup>4</sup>That value was set in the early days of software development in '90, on a workstation HP 9000 equipped with a 100 px wide terminal! Later we continued to keep that value because it does not slow down the solution computing in the selected wavelength range, but ensures a sufficient sampling-density to represent spectra with many interference fringes, provided the step is set to energy.

**the current project .Spj!**

The recommended choice is “`nameBase.1.Spj`”; please note that the software automatically checks for the presence of the extension “`.Spj`”, and adds it if necessary. It can be useful to keep trace of the progress of the characterization by saving milestone projects with names differing in a numerical field only (`2.Spj`, `3.Spj`, ...).

**When one switches the study to a different sample, please restart the software to force a full-reset, otherwise some parameters and options will be inherited from the previous study.**

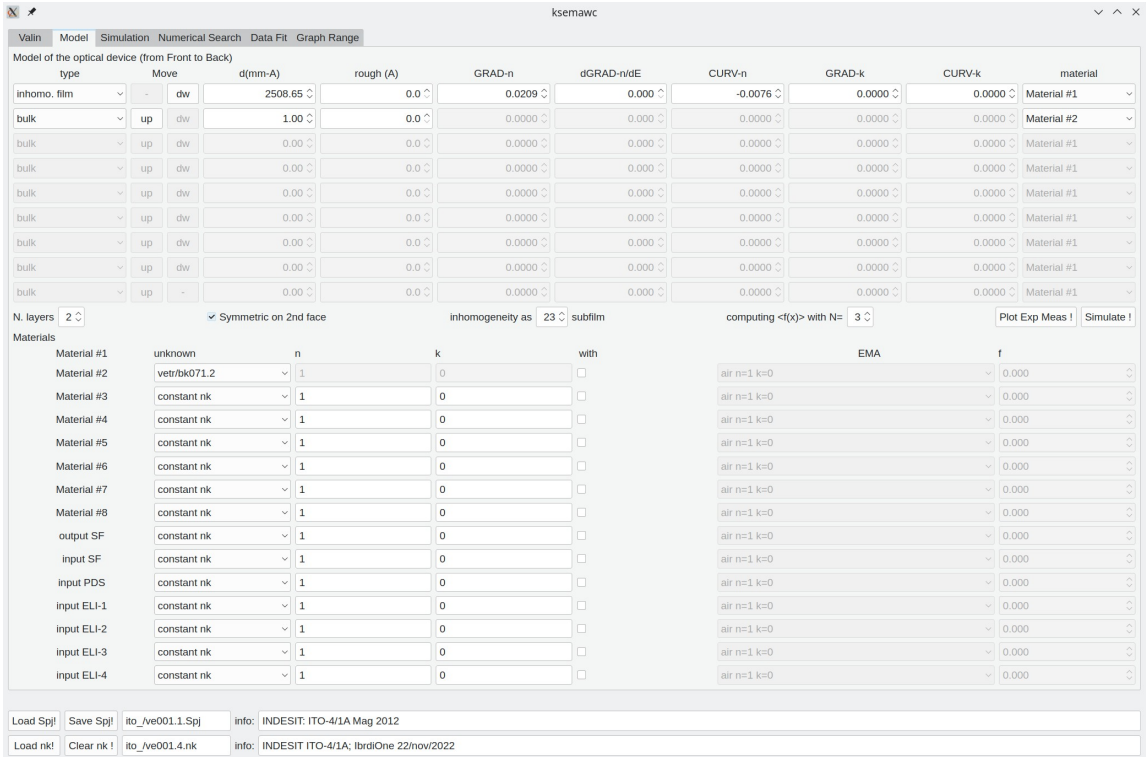


Figure 3: *Model TAB*.

### 3.2 Model TAB

The *Model TAB* (Fig. 3) allows one to model the structure of the optical device.

The first step is setting the layer number (up-to 9) to make an equivalent number of rows, one for each layer, editable.

The first layer on the top corresponds to the one interfaced to air, i.e. the *front* side of the specimen; the bottom interface of the bottom layer is the specimen *back* side. Please note that to attribute *front* and *back* to the two sides of an optical multilayer device is quite arbitrary, except for the case of a thin film deposited on a thick substrate, where *front* normally refers to the coated side of the substrate. Anyway, once it has been established, kSEMAwC considers the two reflectances with extension “rn” and “rp” as obtained with the incident radiation impinging on the *front* side of the specimen: the former at near normal incidence, the latter at oblique incidence in which case the light is polarized. Conversely the reflectance loaded with extension “r1” is assumed to be measured with the radiation impinging on the *back* side, at near normal incidence.

When the absorptance

$$A = 1 - T - R$$

is lower than the experimental error, then “rn” (front) and “r1” (back) reflectances are the same within the experimental error. Otherwise these two measurements are independent and their knowledge is very useful for optimizing the optical model.

Moreover, ellipsometric measurements are intended to be carried out on the *front* side and they have to be not affected by any contribution coming from the *back* side, which usually has to be abraded.

For each layer, the user must set *type*, *thickness* and *roughness*.

In the case of “bulk” layer, e.m. wave propagation is treated by neglecting interference

among the several contributes coming by the two interfaces; layer thickness is in millimetre units.

In the case of “homo. film”, the thickness is expressed in Angstrom units, and it is assumed to be thin, so that the wave propagates in a coherent way; interference phenomena will arise by summing up the contributes coming from the two interfaces.

The same also occurs in the case of “inhomo. film”, but in this case the user can set a parabolic profile for the refractive index across the layer thickness specifying two parameters related to its gradient and curvature. Normalizing the film thickness to 1 (0 on the back and 1 on the front) they are defined as:

$$\begin{aligned}\frac{\Delta n}{\langle n \rangle} &= \frac{n(1) - n(0)}{\int_0^1 n(x) dx} \\ \frac{\langle n \rangle - n(0.5)}{\langle n \rangle} &= \frac{\int_0^1 n(x) dx - n(0.5)}{\int_0^1 n(x) dx}\end{aligned}$$

These parameters are respectively labeled as “GRAD-n” and “CURV-n” in the TAB. Similar parameters and formulas are used for the imaginary part  $k$ .

As a further possibility, by means of the input parameter “d(GRAD-n)/dE” ( $\text{eV}^{-1}$ ) the user can set a linear dependence of “GRAD-n” on the photon energy, so that:

$$\frac{\Delta n}{\langle n \rangle}(E) = \frac{\Delta n}{\langle n \rangle}(0) + qE$$

where  $q$  is the value set as “d(GRAD-n)/dE” and  $\frac{\Delta n}{\langle n \rangle}(0)$  is the one set in “GRAD-n”. We benefited of this further option for characterizing LiF film with many fringes in the UV-VIS-NIR range.

The computation is performed by subdividing the inhomogeneous layer in a number of homogeneous sub-films with refractive index suitably set for modeling the profile; 23 is their default number.

**$n, k$  of the inhomogeneous layer refer to the mean value  $\langle n \rangle$  and  $\langle k \rangle$  as computed along the thickness.**

The effect of roughness for the spectrophotometric measurements is evaluated according to the method described in [2]. More precisely, hemispherical and specular reflectance are respectively evaluated as the statistic average on the roughness ( $\langle \cdot \rangle_\delta$ ) after and before computing the square of the reflectance complex coefficients, that is

$$\begin{aligned}R_{\text{hemispherical}} &= \langle |r(x, y)|^2 \rangle_\delta \\ R_{\text{specular}} &= |\langle r(x, y) \rangle_\delta|^2.\end{aligned}$$

Roughness can be considered as a variation of the film/substrate thickness; its effect is here numerically computed as the mean value on  $2N + 1$  different thickness values, distributed around the Gaussian peak, in the range  $[-3\sigma, 3\sigma]$ . The number of discretization can be set in “computing  $\langle f(x) \rangle$  with N” ( $N = 3$  by default;  $2 \leq N \leq 5$ ).

For the ellipsometric measurements, the above method does not work well; the roughness should be modeled by adding a film with refractive index set to an intermediate value between those of the two materials composing the interface. How to set such a layer in Effective Medium Approximation is explained in the remaining part of this section.

Once sequence and kind (bulk, homo or inhomogeneous) of layers is set, the user has to assign at each layer a material chosen among those listed in Materials (Material #j) in the lower part of the TAB; each material can be set in 5 different ways, by the drop down menu on the left:

1. constant  $nk$ ;
2.  $nk$  by fit option “Fit #M” with  $1 \leq M \leq 7$ ;
3.  $nk$  from one of the  $nk$ -file, previously loaded in *Valin* TAB;
4.  $nk$  computed in the current session within Data Fit TAB.

Please note that Material #1 is reserved to  $nk$  unknown by default. Only when kSEMAWc is used to simulate measurements, the user must assign  $nk$  unknown to one of the known ( $n, k$ ) by surfing to *Simulation* TAB and selecting in the field “Material #1 - nk-unknown - setting of nk-values for simulation” one of the above described options (as an example, the name of one of the  $nk$ -file already set in Valin).

In addition to the 8 materials, the user can set the input medium of the spectrophotometric, PDS (typically  $CCl_4$ ) and ellipsometric measurements, and the output medium of the spectrophotometric ones.

Except Material #1, by ticking the checkbox in the “with” column, the user can set a second material in such a way that  $n, k$  of Material #j are computed according to the Effective Medium Approximation, that is as a mixture of the two materials (the first A on the left, the second B on the right) with volume fractions equal to  $1 - f$  and  $f$  respectively. The value of  $f$  is displayed in the last field of the row. The complex dielectric constant of the composite medium  $\epsilon_e$  is given by the solution of the following equation [5]:

$$(1 - f) \frac{\epsilon_e - \epsilon_A}{\epsilon_A + 2\epsilon_e} + f \frac{\epsilon_e - \epsilon_B}{\epsilon_B + 2\epsilon_e} = 0$$

Please note that to consider an EMA where one of the two materials is the unknown one, the user must insert the unknown material in one additional Material #j with  $j > 1$  to be assigned to the concerned layer of the model instead of Material #1.

The user can quickly check the effect of any change made in this TAB by pushing “Plot Exp Meas !” and then “Simulate !” buttons; the first button pop-up or refresh the windows with the experimental spectra or data plot, while the second draws the simulated curves.

Finally, by ticking the box “Symmetric on second face” the user can set a specular multilayer on the back side of the lower layer. As an example, if the device consists of a thin film on a substrate, this option adds a specular film on the back side of the substrate; if the front film has a growing index profile towards the substrate, the same will hold for the film added to the rear side. That option can be used for substrates treated with sol-gel dipping coating.

**Once a multilayer is set, the layer order can be modified by the “dw” and “up” buttons for each layer. By increasing (+1) the layer number, a new layer is added on the front side; oppositely, by decreasing it (-1), the first layer on the front side is cancelled.**

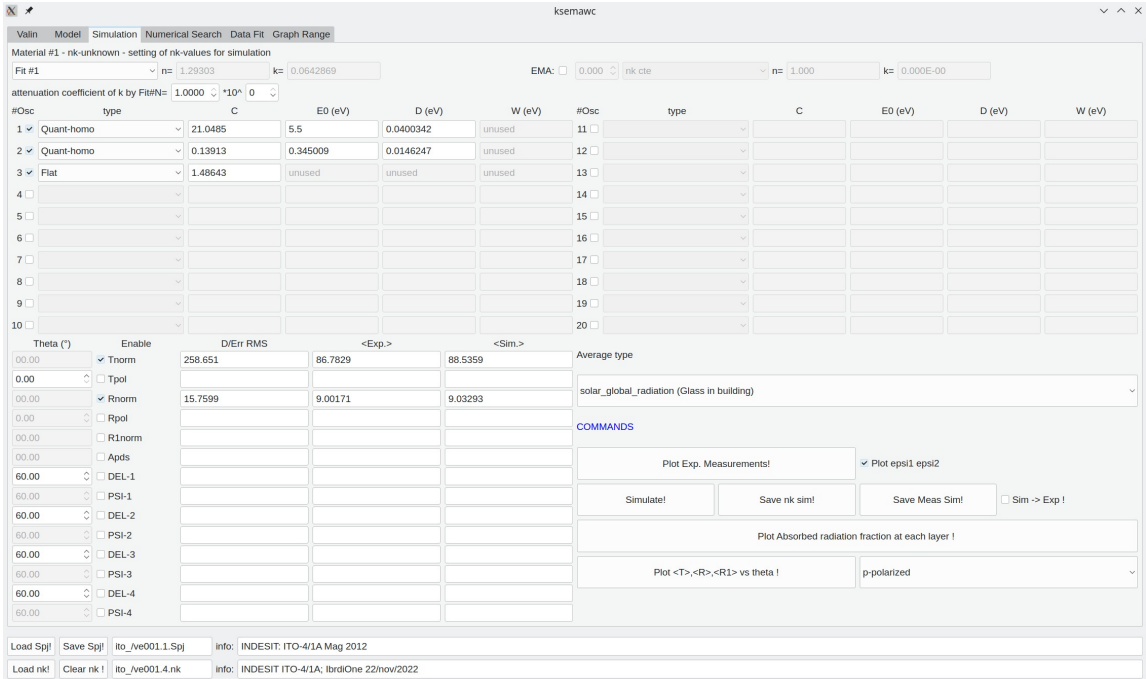


Figure 4: *Simulation TAB.*

### 3.3 Simulation TAB

The *Simulation TAB* (Fig. 4) allows to set the computing of the simulated curves to be compared with the experimental data.

As a first step the user has to set “Material #1 - nk-unknown - setting of nk-values for simulation” in the top of the TAB, in a similar way to what described in the previous section.

If one of the 7 available fit options is selected, the oscillators functions composing it are those signed by a ticked checkbox among the 20 records shown below. Working on these records the user can add new oscillators, modify the current ones or set a totally new fit option. In any case please keep in mind that 20 is the maximum number of available oscillators.

**The same oscillator record should not be shared among different fit options because there is a unique place for storing the parameter values, which depends on the oscillator sequential number and not by the fit option to which it is associated.**

In the drop down menu of each oscillator, the user can choose among 18 typologies:

- Lorentz
- Quant-homo
- Lorentz-Dirac
- Quant-inhom
- Flat

- Drude
- Drude-ionized
- Direct Gap Cody-Lorentzian tail
- Direct Gap Tauc-Lorentzian tail
- Indirect Gap Cody-Lorentzian tail
- Indirect Gap Tauc-Lorentzian tail
- Direct Gap Cody-Urbach (exponential) tail
- Direct Gap Tauc-Urbach (exponential) tail
- Indirect Gap Cody-Urbach (exponential) tail
- Indirect Gap Tauc-Urbach (exponential) tail
- Direct Gap Tauc-Exciton
- Direct Gap Cody-M1M2
- Direct Gap Tauc-M1M2

The detailed description of these oscillators functions and their physical meaning are reported in Appendix A.

Once nk-known has been set, kSEMAWc can compute the curves simulated according to the optical model of the devices already set in the *Model* TAB.

The experimental measurements previously selected in the *Valin* TAB are automatically enabled to be simulated; the user can disable some of them, as well as enable the simulation of some other quantity for which no experimental data are available. Then by pushing “Plot exp. Measures!” a number of windows will pop-up: one for each selected experimental measurement, plus the two  $\lambda$ - $n$  and  $\lambda$ - $k$  with the graphs of  $n(\lambda)$  and  $k(\lambda)$ .

When transmittance and reflectance at near-normal incidence are available, also the absorptance  $A_{front} = 1 - T_{norm} - R_{norm}$  and/or  $A_{back} = T_{norm} + R1_{norm} > 1$  are shown.

Two more windows with the graphs of  $\epsilon_{11}(\lambda)$ ,  $\epsilon_{12}(\lambda)$  (respectively real and imaginary part of the permittivity), will pop-up when the checkbox “Plot  $\epsilon_{11}$   $\epsilon_{12}$ ” is ticked. All these windows are sizable.

**When transmittance and reflectance data are available, a check on their sum is run; if  $T_{norm} + R_{norm} > 1$  and/or  $T_{norm} + R1_{norm} > 1$  a pop-up message informs the user of this anomaly, inviting to check the measurements.**

The scale control of all the plotted graphs is in *Graph Range* TAB, described in 3.6. There the user can also set width and high of the window-graphs at their pop-up, as well as the line thickness. All windows are sizable in runtime.

By pushing “Simulate!”, the simulated curves will be added to the opened graphs as dashed-lines to be distinguishable from the experimental ones, which are drawn as

dot-symbols with error bars. The simulated curves can be saved on hard disk, on a customized location and name, by pushing the button “Save Meas Sim!”. Analogously the nk-values used for the simulation can be saved by pushing the button “Save nk sim !”.

Each time the “Simulate!” button is pushed, both experimental (re-sampled on 201 points) and simulated curves are automatically saved on hard disk in the directory “`expo`” with the names

- `MisSFexp.dat` spectrophotometric experimental measurements (SF)
- `MisSFexpErr.dat` errors of the above ones
- `MisEliexp.dat` ellipsometric experimental measurements (ELI)
- `MisEliexpErr.dat` errors of the above ones
- `MisSim.dat` simulated curves

This make possible to extract the resampled data for further use.

To refreshed the graphs, please push the “Plot Exp. Measurements!”.

The bottom left form is structured as a matrix and reports for each measurements: i) RMS deviation (normalized to the error) between experimental and simulated spectrum (D/Err RMS); ii) mean value, averaged with the spectrum specified in “Average type” combobox, of the experimental spectrum ( $<Exp.>$ ); iii) idem but for the simulated spectrum ( $<Sim.>$ ).

The drop down menu of “Average type” can be easily customized by editing the file `standardSpectra.txt`, located in the folder `kSEMAWc`, where each standard spectrum is described by a couple of lines: the first one contains its name appearing in the combo box menu, the second one the full path in the work folder `Workspace`. The file contained in the distribution is:

```
VIS_10_wl
stnd/media.1
VIS_30_wl
stnd/media.2
VIS_D65
stnd/media.3
solar_10_wl
stnd/media.4
solar_global_radiation
stnd/media.5
DNI_100_wl
stnd/media.6
PWO_scintillation
stnd/pwtdr.1
PWO_scint*APDqe
stnd/pwiqe.1
IEC_60904-3
stnd/IEC60904b3Step5nm.txt
ASTM_G173
stnd/ASTMG173SP.txt
```

```

ISO_9050
stnd/ISO9050.txt
ISO_9845-1
stnd/ISO9845b1.txt
E_891
stnd/E891.txt

```

so that the default menu is:

- VIS 10 wl (Glass in building)
- VIS 30 wl (Glass in building)
- VIS D65 (Glass in building)
- solar 10 wl (Glass in building)
- solar global radiation (Glass in building)
- DNI 100 wl: direct normal radiation
- PWO scintillation
- PWO scintillation \* APDiqe
- IEC 60904-3
- ASTM G173 solar normal direct radiation AM=1.5
- ISO 9050 solar global radiation AM=1.5
- ISO 9845-1 solar normal direct radiation AM=1.5
- E 891 solar normal direct radiation AM=1.5

This list tracks the use (and development!) I made of the software along about 30 years, first dealing with the energy standard for architectural glazings, then the CMS experiment at LHC of CERN, and finally concentrated solar power (CSP). The user is allowed to suppress undesired voices or add new ones.

When the checkbox “Sim → Exp!” is ticked, the simulated values are overwritten on the experimental ones. From that point on the user will work on *synthetic* measurements as if they were *experimental*.

By pushing the button “Plot Absorbed radiation fraction at each layer !” the fraction of the incident light absorbed in each *thin* layer is computed at the incidence angle specified in the “Theta( $^{\circ}$ )” field of  $T_{pol}$  data, and with the polarization chosen in the bottom right combo-box of this Tab. The absorbed radiation spectra are automatically saved in the directory “*expo*” as individual files named **Abs#j.dat**. Actually this feature is limited to devices composed by *thin* layers or where only the first is *bulk* type.

Finally by pushing “Plot  $\langle T \rangle, \langle R \rangle, \langle R1 \rangle$  vs theta”, the graph of mean values averaged over the selected standard spectrum of transmittance, reflectance and back-reflectance versus the incidence angle and for the selected polarization will pop-up; the polarization can be set by its drop down menu (s-polarized, p-polarized and unpolarized).

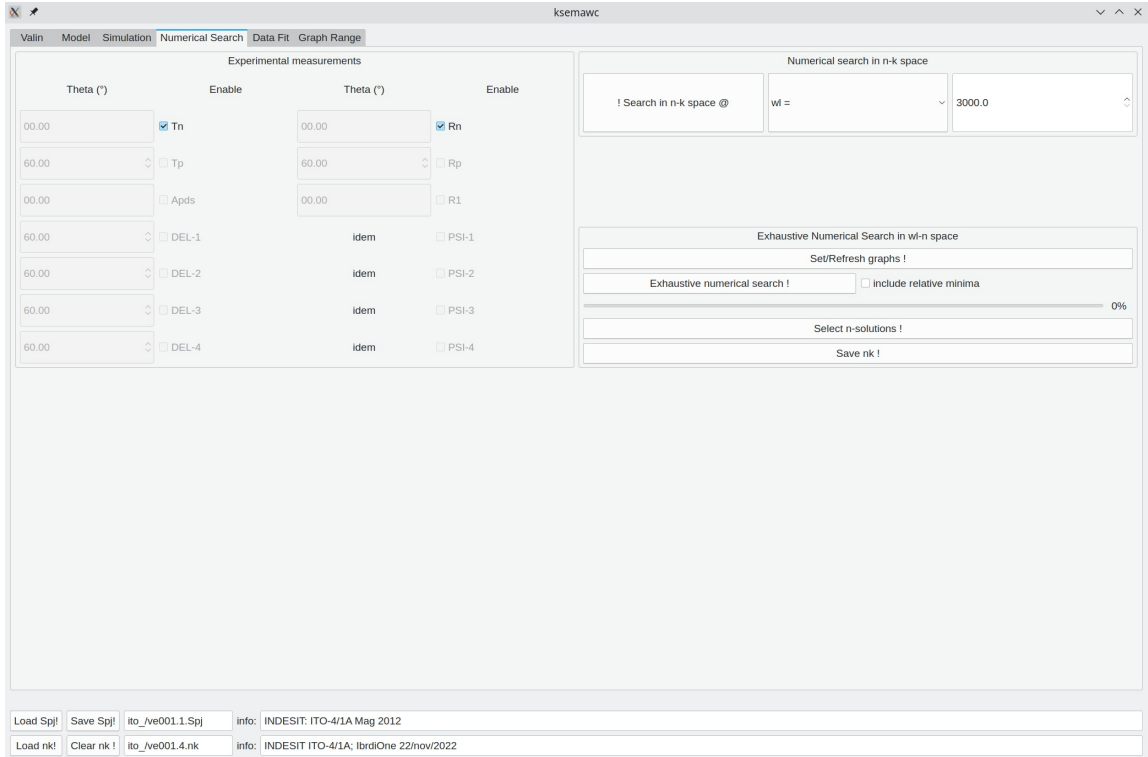


Figure 5: *Numerical Search TAB*.

### 3.4 TAB Numerical Search

One of the methods offered by kSEMAWc for evaluating the complex refractive index of one layer of the optical device is named “Exhaustive Numerical Search”, managed by the *Numerical Search TAB* (Fig. 5).

As outlined in Section 1, before to use this method the user has to set the optical model, including some parameters of the unknown layer like thickness, roughness and possible gradients of the refraction index; under that hypothesis kSEMAWc can numerically search for the  $(n, k)$  couples of values that allow to reproduce the experimental measurements at any given  $\lambda$ . The numerical search of  $n$  is limited to the range of  $n$  selected in the *Graph Range TAB*; differently there are no limits in the search of  $k$ .

More precisely the numerical search is launched by pushing the “Exhaustive Numerical Search !”: from the minimum to maximum wavelength, the solutions  $n_\lambda$  contained in selected  $n$ -range are exhaustively searched by sampling the  $n$  range with 101 points; for each one of these  $n$  values, the  $k$  value that minimize the merit function of Eq. 1 is found. If the merit function is lower than 1 this  $(n, k)$  couple is displayed as a solution with dot and error bar; optionally, when “include relative minima” is ticked, also the relative minima (where the merit function minimum is greater than 1) are considered solutions and plotted as dots. The process is sequentially run over all the wavelengths sampling the wavelength range; a progress-bar informs the user about the status of the process. At the end the found solutions  $n_\lambda$  and  $k_\lambda$  are plotted in two dedicated windows describing a portion of the spaces  $\lambda-n$  and  $\lambda-k$ .

In the case of a thin film, one or more solutions can exist for each wavelength; in addition, the set of solutions is not necessarily connected. By optimizing the model parameters (thicknesses, roughness, gradients, etc.) according to specific guiding crite-

ria [3,4] detailed below, a more connected set of solutions can be obtained; finally, among them, a physically reasonable subset of solutions can be selected and saved. The undesired solutions can be deleted by pushing “Select n-solutions !”: the user will be asked to delimit a polygonal region of the n-plot in which the solutions will be deleted; user has to left-click to add a new point, and right-click to close the polygon. Generally the procedure must be accomplished in several steps. At the end the meaningful  $nk$ -solutions can be saved on the hard disk by pushing “Save nk !”.

A more detailed analysis of the solution search at a given lambda can be performed by pushing the “! Search in n-k space @” button. Here the search is separately performed for each experimental measurement within the region of the  $(n, k)$  space chosen by the user; the search is exhaustive. All these results are graphically displayed as points with y-error calculated on the basis of the experimental error; the sequence of these points with their error delimits the solution-belt in the  $(n, k)$  space. The cross-section of the different belts contains the wanted common  $(n, k)$ -solution of the two or more considered measurements; sometimes multiple crossings (and therefore multiple solutions) are present. To improve the method accuracy it is necessary to choose at least a couple of measurements  $M_1$  &  $M_2$  (as  $T$  &  $R$  or  $\Delta$  &  $\Psi$ ) that gives rise to solution-belts almost orthogonal one to the other in the  $(n, k)$  space.

The top left part of this TAB shows the list of the measurements. By default all the loaded experimental measurements are enabled for the numerical search; the user can modify this choice considering that the Exhaustive Numerical Search method works on two experimental spectra; differently a warning message pops-up and the process is aborted, except in the case of a single enabled measure, where  $n$  is set to value given by the simulation option already chosen while  $k$  is treated as usual. The recommended combination of spectra are  $T$  &  $R$  and  $T$  &  $\Psi$ ; the use of only ellipsometric angles could bring to the over-evaluation of  $k$  being  $\Delta$  strongly affected by roughness.

### **This selection holds even for the *Data Fit* TAB!!!**

The following part of this section gives more detailed information on how to manage the Numerical Search.

The selection of a proper  $n$  range is fundamental for the success of the search; that range can be set in the *Graph Range* TAB. The selection of the  $k$  range is less important because does not affect the numerical search, but just the scale of the  $k(\lambda)$  plot. Coming back to the the *Numerical Search* TAB, two windows will pop-up automatically, or will be refreshed if already opened:  $n(\lambda)$  and  $k(\lambda)$ . Please note that if a reference  $nk$ -file has been loaded (last row of the GUI), its data will be plotted as vertical bars which height corresponds to the error. The graphs will be refreshed by pushing “Set/refresh graphs !”.

Undoubtedly the simplest case is the search of solutions  $(n_\lambda, k_\lambda)$  for a bare substrate: if the  $(n, k)$  search range is suitably sized, the obtained solution will cover the whole wavelength range and appear well connected. The substrate thickness can not be optimised on the basis of the optical measurements, and it must be measured by a calipers or a thickness gauge. A possible problem is an anomalous behaviour of  $n_\lambda$  caused by some measurement imperfection or, more rarely, due to the substrate roughness. Before increasing the model complexity, the user should experimentally verify the presence of roughness, for example by measuring the amount of scattered radiation. Finally, in the case of float glasses, the UV reflectance measured on one side could differ from the one measured on the other side, because the refractive index is a bit different between the

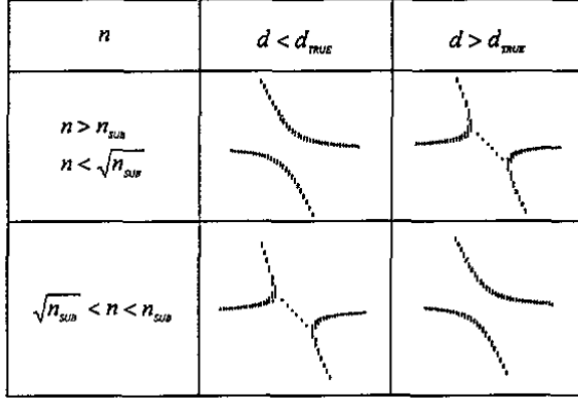


Figure 6: Discontinuity typology affecting the solution crossings related to odd extremes, in the  $\lambda$ - $n$  space, caused by a wrong thickness value.

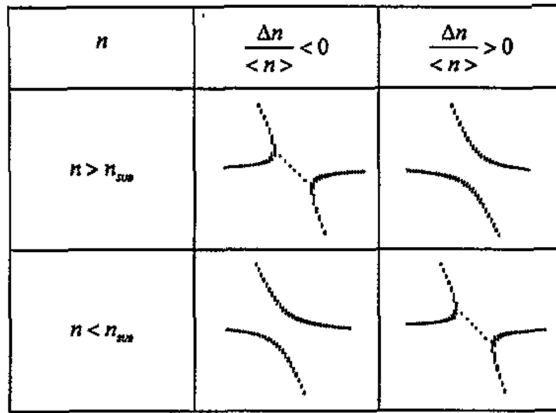


Figure 7: Discontinuity affecting even crossings due to  $n$  gradient.

two sides of the substrate.

The case of thin films is more difficult: the solutions in the  $(\lambda, n)$  space are distributed along branches which draw a sort of *solution crossings*; as a general rule, such crossings are situated in correspondence of even and near odd interference fringe extremes. A simple way to discriminate between even and odd extremes is by drawing the transmittance/reflectance of the bare substrate (in *Simulation TAB* set nk-unknown=nk-substrate): even extremes of reflectance/transmittance fringes are those closer to the bare substrate curve.

At the beginning the model is not optimized and the solution crossings will appear not well connected. The discontinuities can be suppressed or at least reduced by adjusting the model parameters (thickness, roughness, gradient, ecc.). Fortunately, as will be illustrated, the parameters can be optimized according to precise criteria.

The film thickness is the first parameter one should optimize; for low absorption it can be shown [6] that a wrong thickness value can give rise, at the odd crossings, to discontinuities of different types as explained in Fig. 6.

A similar analysis has been performed on thin films with refractive index having a parabolic profile along the thickness [3, 4]; full details are given in the indicated papers, here we just recall some information for the most common case of inhomogeneity for the real part  $n$ .

The gradient of  $n$  mainly affects the even crossings. If that is the case, the user should surf to *Model TAB*, set “inhomo film” (if the actual setting was “homo film”) and adjust the value of  $n$  gradient on the basis of Fig. 7.

The presence of  $n$  curvature is revealed by the impossibility to connect all the odd crossings using the same thickness value. If the examined wavelength range contains both  $m = 1$  and  $m = 3$  crossings, then the true thickness value is between  $d_1$  and  $d_3$ . The user should adjust the curvature value to achieve the simultaneous connection of  $m = 1$  and  $m = 3$  crossing for the same thickness. Please note that  $d_m$ , i.e. the thickness optimized at  $m$  crossing, decreases (increases) for positive (negative) curvature.

Once the solution crossings are well connected, the identification of the solution sub-ensemble having a physical meaning is quite easy. The nonphysical solutions must be deleted by means of the “Selected nk-solutions !” button as already explained. When finished, one has to save them in a *nk*-file, by pushing the button “Save nk !”. As usual the use of `nameBase` followed by a numerical character is strongly recommended; in such a way one can save up-to 10 different *nk*-file concerning to the same specimen. At the beginning of the saving the user will be asked to fill the pop-up field “info” to keep memory about the file.

From this point on the user has two options:

1. to load the found solution file in the *Valin TAB* as  $nk$ -values to be resampled by the internal subroutine of kSEMAWc and be available for the model setting;
2. to load the found solution file at the bottom of the GUI (to be available in Data Fit) and to arrange a suitable composition of oscillators in the *Simulation TAB* for best fitting the  $n$ -values by mean of the specific tools available in the *Data Fit TAB* described in the next section.

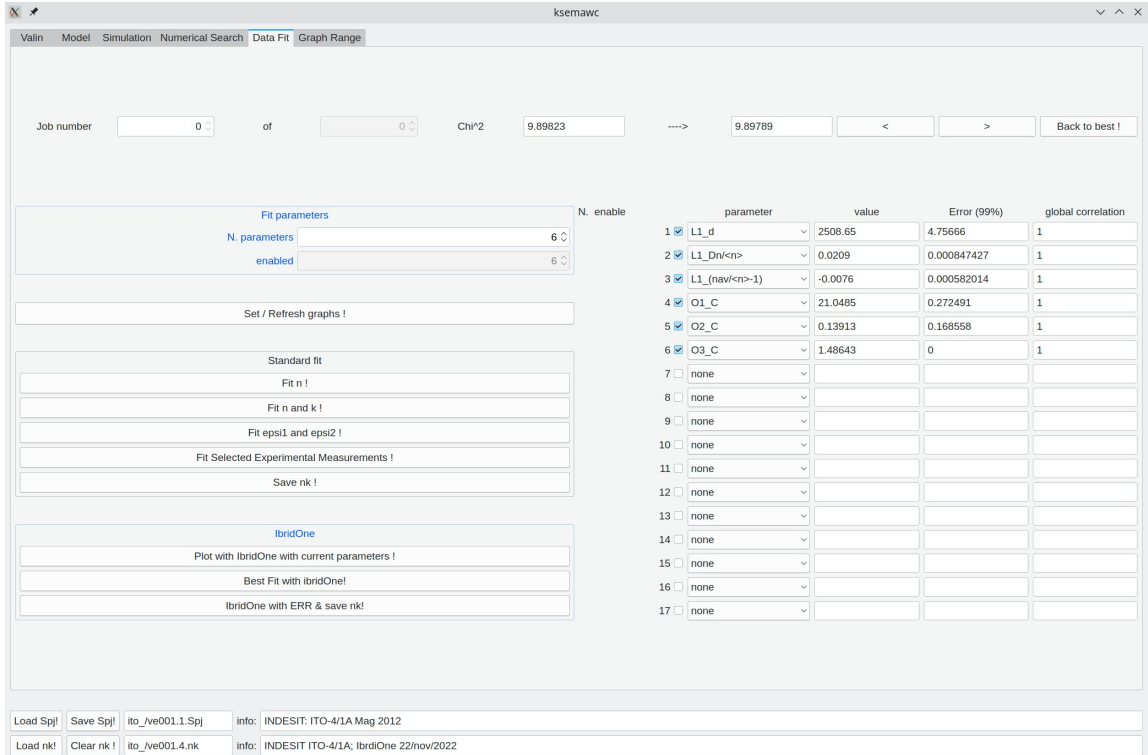


Figure 8: *Data Fit TAB*.

### 3.5 Data Fit TAB

The *Data Fit TAB* (Fig. 8) allows the user to perform several different types of fitting procedures, all based on the minimization of the merit function of Eq. 1 by means of the Levenberg-Marquardt non-linear least square routine, with the purpose to optimize the enabled parameters of the optical model (thickness, roughness, gradient, curvature, ...), as well as of the functions used to describe  $n(\lambda)$  and  $k(\lambda)$  and the dielectric constant.

In the top left part of the box “Fit parameters” the user has to set the total number of parameters to be optimized; this will enable a corresponding number of combo boxes on the right part allowing the user to choose which parameters will be optimized. As soon as one specific parameter is selected, its current value is displayed in the fields in *value* column. The other two fields, *Error 99%* and *global correlation* will be filled at the completion of the first minimization.

On the left, in the box “Standard Fit”, the user can choose one among four standard fit options:

- “Fit n!”, focused on the  $n_\lambda$  data only, i.e.  $k$ -data are not considered;
- “Fit n and k!”, works on  $n_\lambda$  and  $k_\lambda$  data;
- “Fit epsi1 and epsi2!”, works on  $\text{Re}(\epsilon_\lambda)$  and  $\text{Im}(\epsilon_\lambda)$  data;
- “Fit Selected experimental measurements!”.

Except the last option, which works on the selected experimental spectra, the others act on the reference  $nk$ -file (or the epsilon data derived from them) selected at the last row of the GUI, and plotted at the graph refreshing; their purpose is to refine the Fit options

previously selected in the *Simulation TAB*. Please note that if one of the first three fit options is launched, all the parameters concerning the optical model are automatically disabled, i.e. excluded by the best fitting.

The parameters related to the optical model, like thicknesses, roughness, gradients, etc, can be optimized only by means of the last option, the fitting of the experimental spectra as well as the IbridOne method.

The section “IbridOne” allows the user to manage the *IbridOne* method, which name is the synthesis of the words *Ibrido* (i.e. hybrid in Italian) and number *One*, referring to the first version of an innovative hybrid computational method where:  $n(\lambda)$  is modelled by a set of suitable analytical functions (Lorentz, Drude, ecc.) depending on a number of parameters to be optimized; the initial value of these parameters must be good enough to give a first reasonable evaluation of  $n(\lambda)$ . Once  $n_\lambda$  is set,  $k_\lambda$  is numerically evaluated for each  $\lambda$  so that the experimental  $T(\lambda)$  spectrum is perfectly reproduced. With this set of values  $n_\lambda$  and  $k_\lambda$  the software computes the simulated spectrum, and compares it with the experimental one by means of the merit function of Eq. 1. Finally that merit function is minimized by the Levenberg-Marquardt non-linear least square routine to optimize the parameters of the optical model (thickness, gradient, curvature, ...) as well as the enabled parameters of the functions used to describe  $n(\lambda)$ ; please note that at each iteration of the minimization process the whole IbridOne procedure is completely repeated.

As general rule any kind of Reflectance spectrum, as well as any ellipsometric  $\Psi$  spectrum can be used in IbridOne, while a transmittance spectrum is always needed for the numerical computation of  $k_\lambda$  at each sampled  $\lambda$ . Please note that by definition the transmittance spectrum is always perfectly reproduced.

***IbridOne* can be used only after a suitable Fit#j option has been set in the *Simulation TAB* (see section 3.3). Moreover in the *Numerical Search TAB* the user must tick a couple of measurements: one transmittance (mandatory) and at least one reflectance /  $\Psi$ .**

**Approaching a new material, running first the *Numerical Search* and selecting a reasonable solution set having physical meaning is recommended in order to choose the most proper functions for modeling  $n(\lambda)$ .**

Another preliminary operation is to verify the suitability of the  $n$  and  $k$  ranges (set in *Graph Range TAB*) where solutions will be searched. Then, by surfing to the *IbridOne TAB*, three windows containing the plots of  $n(\lambda)$ ,  $k(\lambda)$  and  $R(\lambda)$  or  $\Psi(\lambda)$  (according to the one selected in the *Numerical Search TAB*) will pop-up or will be refreshed. In any case by pushing the “Set/Refresh graphs !” button, these windows will be refreshed. If the checkbox “Plot epsi1 epsi2” has been ticked in the *Simulation TAB*, other two windows with the plots of  $\epsilon_1(\lambda)$  and  $\epsilon_2(\lambda)$  will be shown/refreshed. Once again, please verify the ranges for  $\epsilon_1$  and  $\epsilon_2$  in the *Graph Range TAB*.

By pushing the “Plot with ibridOne with current parameters !” button, a single computing run of IbridOne is launched, with the fit option already set, on the basis of the current parameter values, without optimization; the results are shown as new  $n(\lambda)$ ,  $k(\lambda)$  and  $R/\Psi(\lambda)$  curves in the opened windows. Moreover each graph will include the  $(n_\lambda, k_\lambda)$  reference solutions and the experimental  $R_{exp}(\lambda)$ .

The “Best Fit with ibridOne!” button launches the IbridOne procedure together with

the best fitting of the parameters listed in the “parameter” column and enabled by ticking the “enabled’ checkbox. As already explained, the user has to set the displayed parameters by the individual drop-down menu, while their total number is set by the spin box “N. parameters”

**IbridOne can be launched only if at least one parameter has been enabled for the best-fitting.**

Once satisfactory results are obtained, by pushing the “IbridOne with ERR & save nk!” button,  $nk$  values and their error (based on the experimental errors) are computed, provided that at least one parameter is left free to be optimized; otherwise errors are not evaluated. The user will be asked to choice a filename and to input an informative comment about the file is going to be saved on the hard disk.

The two buttons “<” and “>” on the top-right allow to browse the jobs run in the current session. The user can also directly go back to the job having the lowest merit function by pushing “Back to best!”.

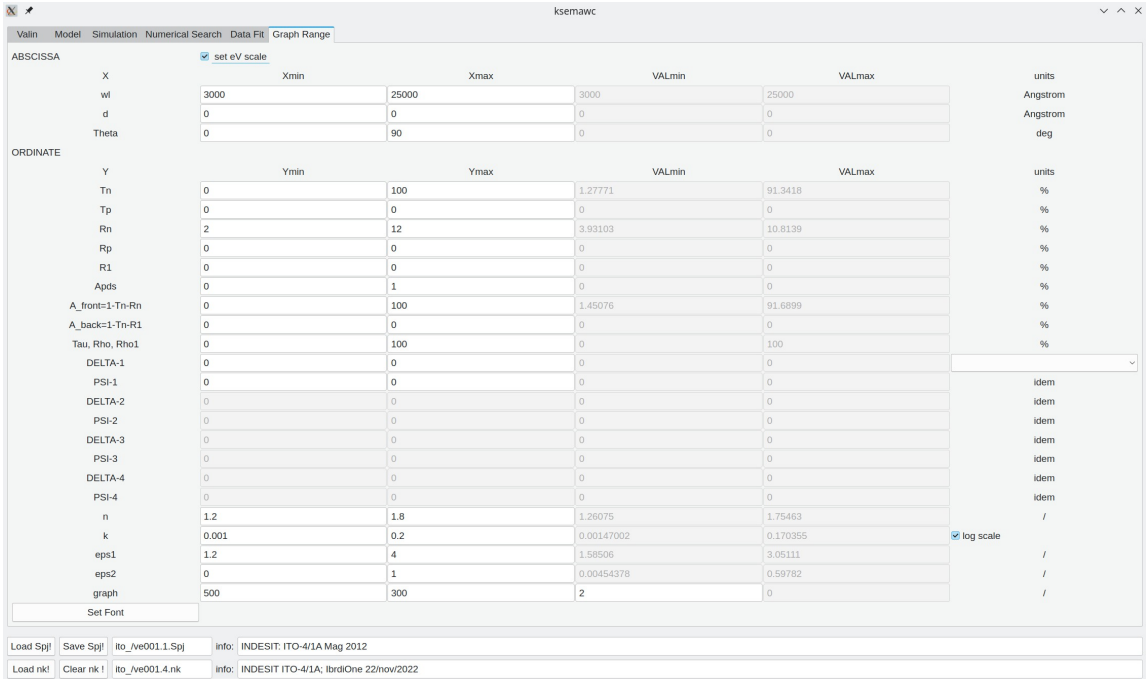


Figure 9: *Graph Range TAB*.

### 3.6 Graph range TAB

The *Graph Range* TAB (see Fig. 9) is dedicated to the graph window control.

On the top of this TAB, on the right of “ABSCISSA”, the checkbox “set eV scale” controls the abscissa: when ticked the unit is eV, otherwise is Å. Please note that this choice is completely independent by the step used to re-sample measurements and *nk*-file loaded in the *Valin* TAB.

The *Graph Range* TAB has 4 columns of fields; except for the last row, only the values in the first two columns can be edited, to set minimum and maximum values of the scale used in the respective graphs. The values reported in 3rd and 4th columns are the minimum and maximum of the loaded data.

Only for the graph of the imaginary part of the complex refractive index the user can enable the logarithmic scale by ticking the box at the end of the row.

Differently from all the others, the last row has three editable fields (the fourth is not used) with the following graph parameters:

- width (pixels) at the window pop-up
- height (pixels) at the window pop-up
- line thickness.

To make the new values of width and height at window pop-up effective, the user has to save the project and restart the program; anyway please note that qwt-plot windows can be manually resized in run-time. For all the other settings, the opened graphical windows will be refreshed when the focus will go back to any another TAB.

Finally font and character dimension of the GUI can be changed by pushing the button “Set Font”. After that the user should resize the GUI to optimize its visualization. These options will be automatically saved when the software is stopped by clicking the top right closure button of the GUI window; they are restored at the next launch of the software.

## 4 Mini-guide to the characterization procedure

In order to facilitate the use of kSEMAWc, this section describes a recommended sequence of operations / checks that allows one to obtain a reliable characterization of samples. Later, once the user becomes familiar with the software and above all with the topic, he will have the opportunity to define his own procedure, perhaps specific for a given family of samples.

- Check that the measured spectra have no artifacts (such as an abrupt discontinuity) and that the sum of transmittance and reflectance (measured under the same incidence angle) is below 100%.
- Set experimental spectra (measurements) and *nk*-files in the *Valin* TAB and save the project. In the case of hemispherical measurements, tick the appropriate field. If necessary, specify the spectrum of the reference sample and tick the appropriate field to multiply the reflectance spectra for the reference one, during the data upload.
- Set the model in the *Model* TAB starting from the simplest hypothesis (substrate, homogeneous film, etc.).
- Surf to the *Simulation* TAB and plot the experimental measurements. To get an idea of the refractive index value, select “constant nk” from the nk-unknow menu and, by trial and error, try to reproduce the spectrum in a low absorption region (usually toward the NIR energy range). If necessary, adjust the thickness of an eventual thin film.
- Surf to the *Graph Range* TAB and set the ranges of *n* and *k* over which the numerical search for solutions has to be run. **Warning: the search intervals coincide with the *n* and *k* graphs scale!** If necessary, adjust the vertical axis scale of those plots.
- Surf to the *Numerical Search* TAB and tick the measurements you intend to use in the numerical search; in the case of a thin film, it is recommended to start with only two spectra (typically transmittance and reflectance measured on the front side) because this allows one to more easily understand the types of discontinuities that will be eventually observed. In the case of thin films, to make easier the recognition of the kind of discontinuity, thick the checkbox “include relative minima”.
- Select a wavelength  $\lambda_0$  towards the NIR (as an example wlMAX) taking care that it is not too close to an interference peak/valley. Launch the command “! Search in n-k space @”. If the search range has been correctly set, two solution bands will be drawn; their intersection contains the sought solution. If not, adjust the search area in the space (*n*, *k*) until an intersection is found.
- Push the button “Exhaustive numerical search!” to found and plot all solutions having *n* within the selected  $\lambda$ -*n* space.
- **For substrates:**, once solutions over the full spectral range have been obtained, push the button “Save nk !” to save permanently them on the hard disk with a suitable name. It is recommended to fill the field “info:” with the basic information that will help to remember the meaning of the files in the future.

**For thin films:** in order to obtain connected solutions, it will be necessary to carefully optimize the optical model, by adjusting the thickness and possibly introducing gradient / curvature and / or roughness. The solutions without physical meaning should be deleted by pressing “Select n-solutions !”, maybe in several steps. Once reasonably connected solutions are obtained, these have to be saved as described just above.

- Inevitably the solution trend in the  $\lambda$ - $n$  space will present anomalies due to measurement errors and, in the case of thin films, to the intersections between solution branches. In order to obtain a more regular behavior, the user should surf to *Simulation TAB* and set-up a fit option consisting of a suitable number of oscillators, preferably selected on the basis of physical criteria related to the material under investigation. By pressing “Plot exp. measures!” and then “Simulate!” the user can adjust all the parameters of the selected oscillators to get reasonable initial values.
- Surf to the *Data Fit TAB*, make all the parameters of interest of the previously configured fit option visible, enable a number of them for best fitting, push “Set/Refresh graphs !” and then use one of the four options to fit  $n$ ,  $n$  and  $k$ ,  $\tilde{\epsilon}(\lambda)$  or the experimental data. We recommend to start the best-fit with just a few enabled parameters, and then gradually include all the others to be optimized.
- For dielectric materials or when the transmittance spectrum cannot be satisfactorily reproduced, the IbridOne procedure can be launched by pressing the button “Best Fit with IbridOne!”. This will perfectly reproduce the  $T(\lambda)$  data and will optimize all the parameters of interest of the fit option and of the optical model (such as thickness, gradient, curvature, etc) to fit the other selected measurements ( $R(\lambda)$  for example). Once again one should start the procedure by enabling just a few parameters, and then gradually include all the others in the optimization process. Once the result is satisfactory, push “IbridOne with ERR & save nk!” for computing and permanently saving the solutions on the hard disk.

Finally, we suggest the accurate reading of the paper [7] where several examples of the use of kSEMAW are presented.



## A Oscillators expressions

Up to now we have described the light propagation in multilayers using the wavelength  $\lambda$  and the refractive index  $n - ik$  as independent variables. To describe the interaction of photons with matter it is instead more convenient to use the photon energy  $E = h\nu = \hbar\omega = hc/\lambda$  and the relative permittivity  $\epsilon_1 - i\epsilon_2$ .

Refractive index and permittivity are both complex quantities connected by the equations

$$\epsilon_1 = n^2 - k^2, \quad \epsilon_2 = 2nk.$$

and inversely

$$n = \frac{1}{\sqrt{2}} \sqrt{\sqrt{\epsilon_1^2 + \epsilon_2^2} + \epsilon_1}, \quad k = \frac{1}{\sqrt{2}} \sqrt{\sqrt{\epsilon_1^2 + \epsilon_2^2} - \epsilon_1}. \quad (2)$$

Generally the theories for the light-matter interaction give simpler expressions for the permittivity or, more precisely for the complex dielectric susceptibility  $\tilde{\chi} = \chi_1 - i\chi_2$ . Dielectric susceptibility and permittivity are connected by the simple equation:

$$\tilde{\epsilon} = \epsilon_1 - i\epsilon_2 = 1 + \tilde{\chi} = 1 + \chi_1 - i\chi_2. \quad (3)$$

The 1 term in Eq. 3 takes into account the vacuum permittivity  $\epsilon_0$ .

Optical data analysis is often performed by best-fitting, optimizing the parameters of some functions modelling  $n(E)$  and  $k(E)$  or  $\chi_1(E)$  and  $\chi_2(E)$ . Even if these functions may be in principle arbitrary, it is much more convenient that they possess a simple physical interpretation and are compatible with the Kramers-Kronig relation which connect the real and imaginary part of the susceptibility:

$$\chi_1(E) = \frac{2}{\pi} \mathcal{P} \int_0^\infty \frac{\chi_2(X)X}{X^2 - E^2} dX \quad (4)$$

In this appendix we describe some useful analytical expressions and numerical procedures used to calculate susceptibility values (and thereafter refractive index values) which satisfy both these requirements.

In the current version, kSEMAWc can model the dependence of the refractive index on wavelength  $n(\lambda)$  with 7 different fit options; each option can be built using up to 20 oscillators belonging to the following 18 classes:

- Lorentz
- Quant-homo
- Lorentz-Dirac
- Quant-inhom
- Flat
- Drude
- Drude-ionized
- Direct Gap Cody-Lorentzian tail

- Direct Gap Tauc-Lorentzian tail
- Indirect Gap Cody-Lorentzian tail
- Indirect Gap Tauc-Lorentzian tail
- Direct Gap Cody-Urbach (exponential) tail
- Direct Gap Tauc-Urbach (exponential) tail
- Indirect Gap Cody-Urbach (exponential) tail
- Indirect Gap Tauc-Urbach (exponential) tail
- Direct Gap Tauc-Exciton
- Direct Gap Cody-M1M2
- Direct Gap Tauc-M1M2

Once the user sets a fit option, kSEMAWc will calculate the total  $\tilde{\epsilon}$  adding up the susceptibilities of all the selected oscillators: the *Flat* oscillator will take into account the “1” in Eq. 3. The complex refractive index will be then calculated using Eq. 2.

For each selected oscillator the user has to fill the parameter boxes. The oscillators (with the exception of the **Flat** and **Direct Gap Tauc-Exciton** ones) are normalized in the sense that they are proportional to an intensity parameter  $C$  which can be correlated to the electron density involved in the transitions.

This normalization has been made starting from a general sum rule on  $\epsilon_2$  which states:

$$\int_0^\infty \epsilon_2(E) EdE = \frac{\pi(\hbar q)^2 N_e}{2\epsilon_0 m_e} = \frac{N_e}{4.61706 \cdot 10^{20}} eV^2 \quad (5)$$

where  $N_e$  is electron number per unit volume of the material (all of them, including the core electrons),  $q$  is the electron charge and  $m_e$  is the electron mass.

The sum rule is based on a linear expression of  $\epsilon_2$  and therefore if we build  $\epsilon_2$  as a sum of terms corresponding to transitions starting from different groups of electron states we could imagine that each term can be normalized to the corresponding electron number. This is not exactly true but it is used in kSEMAW as a good first approximation which gives to  $C$  a clear physical meaning. Therefore for each oscillator the  $C$  value is chosen so that it satisfy with the the best possible approximation the following expression:

$$\int_0^\infty \epsilon_2^{osc}(E) EdE = C$$

The equation is exactly satisfied by the Lorentz, Drude and Quant-inhomo oscillators while it is only approximately valid for the other ones.

The  $C$  value can be therefore interpreted as:

$$C = \frac{\pi(\hbar q)^2 N_e^{osc}}{2\epsilon_0 m_e}$$

For a given material the total  $N_e$  value can be evaluated as:

$$N_e = \frac{\rho}{M} Z_e N_a$$

where  $\rho$  is the material density,  $M$  is its molar mass,  $Z_e$  is the number of electrons in the base molecule and  $N_a$  is the Avogadro's number ( $6.022 \cdot 10^{23}$ ).

To get an idea about a typical order of magnitude of  $C$  coefficients, let us consider the case of silicon where we have  $\rho = 2.329 \text{ gr/cm}^3$ ,  $M = 28.086$ ,  $Z_e = 14$  and therefore  $N_e = 6.991 \cdot 10^{23} \text{ cm}^{-3}$  and:

$$\int_0^\infty \epsilon_2(E) E dE = 1515 \text{ eV}^2$$

The valence band contains 4 electrons per atom and therefore its contribution to  $\epsilon_2(E)$  should be built using oscillators equivalent to about  $2 \cdot 10^{23} \text{ cm}^{-3}$  or in other words corresponding to an integrated value of  $433 \text{ eV}^2$ .

## A.1 Lorentz oscillator

The “Lorentz” oscillator is based on the classic Lorentz oscillator formulas [8]

$$\begin{aligned} \tilde{\chi} &= \frac{C}{\pi D E'_0} \left[ \frac{D}{E'_0 - E + iD} + \frac{D}{E'_0 + E - iD} \right] \\ \chi_1 &= \frac{2C}{\pi} \frac{(E_0^2 - E^2)}{(E_0^2 - E^2)^2 + (2ED)^2}, \quad \chi_2 = \frac{2C}{\pi} \frac{2ED}{(E_0^2 - E^2)^2 + (2ED)^2} \end{aligned}$$

where  $C = (\pi \hbar^2 q^2 N)/(2m\epsilon_0)$  is the oscillator amplitude<sup>5</sup> with dimensions [ $\text{eV}^2$ ],  $E_0^2 = E_0'^2 + D^2$  is the resonance energy while  $D$  is the line width; these two last parameters are expressed in eV.  $D$  is related to the excited state lifetime  $\tau$  by  $2D = \hbar/\tau$

If  $k \ll n$  these formulas give the approximate behaviour of  $n(\lambda)$  described by the Sellmeier formula.

## A.2 Homogeneous quantum oscillator

The “Quant-homo” oscillator is based on the simple quantum oscillator formulas [9] valid for the case of homogeneous broadening:

$$\begin{aligned} \tilde{\chi} &= \frac{C}{\pi D E_0} \left[ \frac{D}{E_0 - E + iD} \right] \\ \chi_1 &= \frac{C}{(\pi D E_0)} \frac{(E_0 - E)/D}{1 + [(E_0 - E)/D]^2}, \quad \chi_2 = \frac{C}{(\pi D E_0)} \frac{1}{1 + [(E_0 - E)/D]^2}. \end{aligned}$$

The meaning of the parameters  $C$ ,  $E_0$ ,  $D$  is the same as in the Lorentz case. The difference between Lorentz and quantum oscillators is shown in Fig. 10 where 1 was added to the susceptibility to get the permittivity.

As reported in [10], the “Quant-homo” oscillator formula is obtained by neglecting a not-resonant term in the quantum treatment (otherwise a formula practically equivalent to the Lorentz oscillator would be obtained). As shown in Fig. 10 this approximation is excellent near the resonance energy while a small difference appears far away from it. On the other hand the simple and elegant equations of the quantum oscillator allow one to obtain analytical expressions when the oscillator is used to make convolutions in materials with a continuous distribution of density of states.

---

<sup>5</sup>where  $N$  is the carrier density,  $q$  is the electron charge,  $m$  is the electron mass and  $\epsilon_0$  is the vacuum dielectric constant.

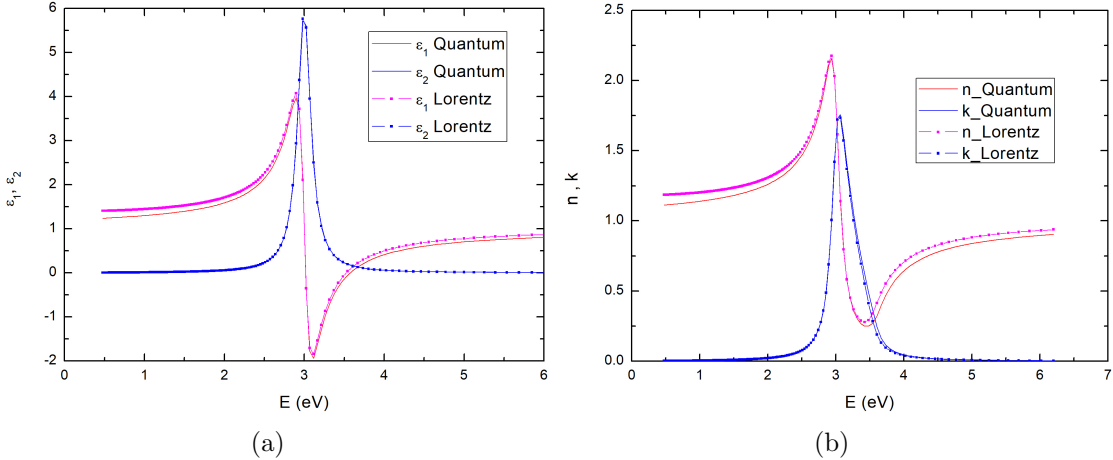


Figure 10: Behaviour of  $\epsilon_1, \epsilon_2$  (a) and of  $n, k$  (b) for quantum and Lorentz oscillators with  $C=5.6 \text{ eV}^2$ ,  $E_0 = 3 \text{ eV}$ ,  $D=0.1 \text{ eV}$ .

### A.3 Lorentz-Dirac oscillator

This oscillator can be derived writing for the classical electron dynamics an equation very similar to that used for the Lorentz oscillator but adding to the usual elastic restoring force and viscous damping terms a term similar to the radiation-reaction force given by  $mt_0\dot{a}$  [11]:

$$m\ddot{r} + m2\Gamma_0\dot{r} + m\omega_0^2 r = -eE_{loc} + mt_0\ddot{r}$$

if  $t_0 = q^2/(6\pi\epsilon_0 mc^3)$  this equation is equal to the Lorentz-Dirac equation of motion for a charged particle under the influence of an external force as well as its own electromagnetic field, but for the use in  $\tilde{\chi}$  fitting  $t_0$  is considered a free parameter.

Substituting  $E_{loc} = E_0 e^{i\omega t}$  and  $r = ze^{i\omega t}$  and using the expressions  $P = -qr = \alpha E$  and  $\tilde{\chi} = N\alpha/\epsilon_0$  one obtains:

$$\tilde{\chi} = \frac{Nq^2}{\epsilon_0 m} \frac{1}{(\omega_0^2 - \omega^2 + i\omega 2\Gamma_0 + it_0\omega^3)}$$

Normalizing the oscillator as before the equations used in the code are:

$$\chi_1 = \frac{2C}{\pi} \frac{(E_0^2 - E^2)}{(E_0^2 - E^2)^2 + (2ED + E^3/W)^2}, \quad \chi_2 = \frac{2C}{\pi} \frac{2ED + E^3/W}{(E_0^2 - E^2)^2 + (2ED + E^3/W)^2}$$

where  $C = (\pi\hbar^2 q^2 N)/(2m\epsilon_0)$  is the oscillator amplitude,  $E_0^2$  is the resonance energy,  $D = \hbar\Gamma_0$  and  $W = \hbar/t_0$  (with dimensions eV).

It can be seen that this version of the Lorentz-Dirac oscillator can be interpreted as a Lorentz oscillator with an energy dependent broadening parameter  $\Gamma(\omega) = \Gamma_0 + t_0\omega^2/2$  increasing at large energies as  $\omega^2$ . It must be also noted that if we put  $\Gamma_0 = 0$  and we use the Dirac value for  $t_0$  we obtain for an optical line a broadening corresponding to a lifetime of the order of  $10^{-8}$  s as expected for a radiation damping term alone.

The Lorentz-Dirac oscillator used in kSEMAW is not exactly equal to that used in the literature. In the version used in the literature [11] the term  $t_0\dot{a}$  is replaced by  $-q/mE_{loc}$  because this substitution avoids any problem (runaway and preacceleration solutions) which could arise for external fields with very fast variations. On the other hand the literature version is not compatible with the sum rule (the integral diverges).

The kSEMAW version is instead compatible with the sum rule since for large energies  $\chi_2$  decreases as  $E^3$  and it can be shown that the unphysical behaviors are not expected for incident radiation with a wavelength much larger than the classical electron radius [12]. The two versions give very similar results for not too large  $t_0$  values and are practically identical for narrow peaks.

It is reported that the Lorentz-Dirac oscillator can give a very good fit of the optical constants of noble metals [13, 14]. It was also preferred to the simple Lorentz oscillator for the fit of the  $\tilde{\epsilon}$  of crystalline silicon [15, 16] because the Lorentz oscillator has a wide tail at low energies giving an exaggerated absorption below the fundamental absorption edge [17] while the asymmetrical Lorentz-Dirac oscillators has a faster  $\epsilon_2$  decay at low energies.

#### A.4 Inhomogeneous quantum oscillator

When the absorbing centres in a material cannot be considered as identical replicas, the absorption-line broadening is inhomogeneous. For example absorbing centres may be slightly different in a crystal because of the random presence of strain or proximity to other lattice defects and impurities that are randomly distributed or in a polycrystalline material because of the random orientations and sizes of the grains. The “Quant-inhomo” oscillator formula is therefore obtained by making the convolution between a homogeneous quantum oscillator and a Gaussian distribution centred in  $E_0$  and with half width at half maximum (HWHM) equal to  $D$  [18]; the line width of the homogeneous quantum oscillator is assumed to be much lower than the Gaussian one. The complex susceptibility is given by:

$$\tilde{\chi} = \frac{C}{K} \left\{ D_+ \left( \frac{E_0 - E}{D'} \right) - i \cdot \exp \left[ - \left( \frac{E - E_0}{D'} \right)^2 \right] \right\}$$

where  $D_+$  is the Dawson function,  $D' = D/\sqrt{\ln 2}$  and the normalization constant  $K$  is given by:

$$K = \int_0^\infty E \cdot \exp \left[ - \left( \frac{E - E_0}{D'} \right)^2 \right] dE = \frac{D'^2}{2} \exp \left( - \frac{E_0^2}{D'^2} \right) + \frac{E_0 D' \sqrt{\pi}}{2} \operatorname{erfc} \left( - \frac{E_0}{D'} \right)$$

#### A.5 Flat oscillator

The “Flat” oscillator is a simple constant term:

$$\epsilon_1 = C^2, \quad \epsilon_2 = 0.$$

It has to be noted that in this special case the  $C$  value is squared to obtain  $\epsilon_1$  so that  $C$  corresponds the refractive index offset generated by this “Flat” oscillator:  $n = C + \dots$

**A “flat” oscillator with  $C > 1$  must be always inserted into every option fit to take into account the vacuum permittivity  $\epsilon_0$  as well as the tail-contribute of some transitions at high energies, out of the investigated wavelength range, and not explicitly considered.**

## A.6 Drude oscillator

The “Drude” oscillator is based on the formulas which describe the response of a free electron gas:

$$\chi_1 = -\frac{2C}{\pi} \frac{1}{D^2 + E^2}, \quad \chi_2 = \frac{2C}{\pi} \frac{D}{E(D^2 + E^2)}.$$

In this case  $D$  is related to the carrier scattering time  $\tau$  by  $D = \hbar/\tau$  while  $C$  is given by  $C = (\pi\hbar^2 q^2 N)/(2m^* \epsilon_0)$  where  $N$  is the carrier density per unit volume and  $m^*$  is their effective mass.

With this definition of  $C$  the Drude oscillator exactly satisfy the sum rule since:

$$\int_0^\infty \frac{2CD}{\pi E(D^2 + E^2)} EdE = \frac{2CD}{\pi} \int_0^\infty \frac{1}{(D^2 + E^2)} dE = \frac{2CD}{\pi} \left[ \frac{1}{D} \arctan \left( \frac{E}{D} \right) \right]_0^\infty = C$$

in agreement with Eq. 5.

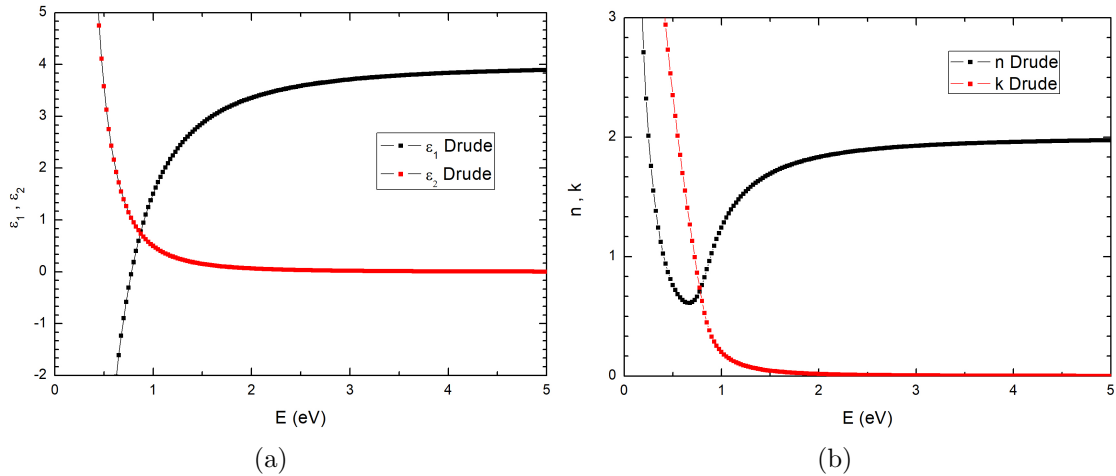


Figure 11: Behaviour of  $\epsilon_1, \epsilon_2$  (a) and  $n, k$  (b) for a Drude oscillator ( $C = 4.074 \text{ eV}^2$ ,  $D = 0.2 \text{ eV}$ ,  $\epsilon_\infty = 4$ ).

Complex refractive index and complex dielectric constant as a function of energy are shown in Fig. 11. To obtain a reasonable permittivity a constant equal to 4 has been added to the susceptibility. This offset, generally called  $\epsilon_\infty$ , is larger than 1 to take into account the tail-contribute of high energy oscillators, as explained previously.

An important energy value is the longitudinal plasma energy i.e. the energy for which  $\epsilon_1 = 0$ . This energy is given by  $E_p^2 = 2C/(\pi\epsilon_\infty) - D^2$  and it is located between the minimum and the flex in  $n(E)$ . Therefore we can shift the  $n(E)$  minimum by changing  $C$ , but this will also affect the behaviour at low energies. When  $E$  approaches zero, both  $n$  and  $k$  diverge. For  $E \ll D$ ,  $n \simeq k \simeq \sqrt{C/(\pi ED)}$ .

In textbooks it is often stated that at short wavelengths the absorption coefficient increases like  $\lambda^2$ , which is equivalent to say that  $k(\lambda)$  increases like  $\lambda^3$ . This approximated behaviour can be obtained from the relation  $\epsilon_2 = \chi_2 = 2nk$  supposing that  $n$  is nearly constant. In this case, if  $E \gg D$ , we have that  $k = CD/(\pi n E^3)$ .

This behaviour is visible in Fig. 12, showing  $n(\lambda)$  and  $k(\lambda)$ , below 1000 nm; conversely for longer wavelengths the minimum in  $n(\lambda)$  completely modifies the behaviour giving a nearly linear increase.

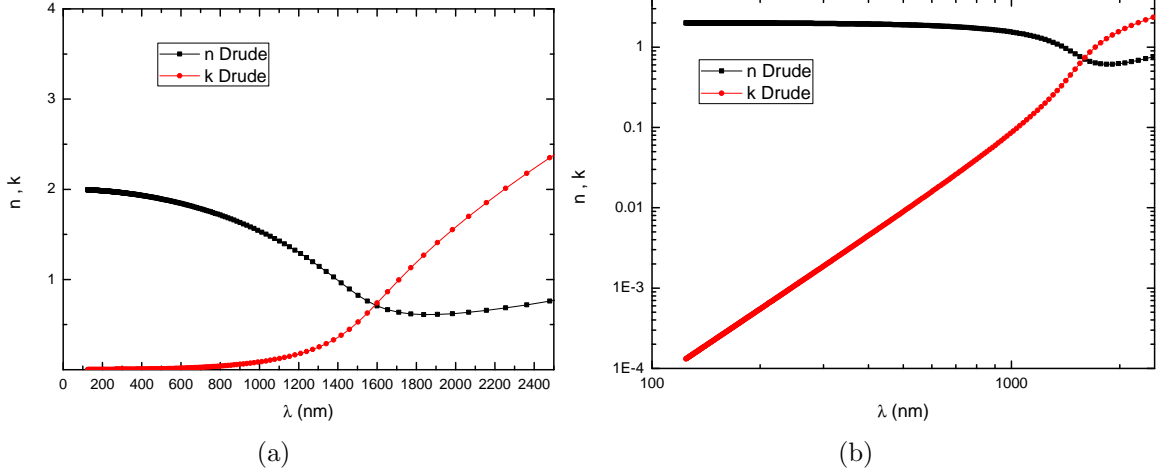


Figure 12: Linear (a) and double logarithmic (b) plot of  $n, k$  versus  $\lambda$  for a Drude oscillator ( $C = 4.074 \text{ eV}^2 \text{ eV}$ ,  $D=0.2 \text{ eV}$ ,  $\epsilon_\infty = 4$ ).

The Drude oscillator is typically used to fit the optical constants of TCOs. An example for a typical ITO is contained in ref. [19] where  $E_p = 0.78 \text{ eV}$ ,  $\epsilon_\infty = 4$ ,  $D = 0.2 \text{ eV}$  are found and therefore  $C = 4.074 \text{ eV}^2$  is deduced. If the carrier effective mass is known ( $m^* = 0.35m_e$  for ITO [19]) the carrier concentration can be obtained from  $C$  by using:

$$N(\text{cm}^{-3}) = C(\text{eV}^2) \frac{m^*}{m_e} 4.617 \cdot 10^{20};$$

with the previously given numbers we get  $N = 6.58 \cdot 10^{20} \text{ cm}^{-3}$  for that material.

Moreover the optical mobility can be calculated from  $D = \hbar/\tau$  using the equation  $\mu = q\tau/m^*$ . Numerically we have:

$$\mu\left(\frac{\text{cm}^2}{\text{Vs}}\right) = \frac{1.159}{D(\text{eV})m^*/m_e}$$

with the previously given numbers we get  $\mu = 16.5 \text{ cm}^2/(\text{Vs})$  for that material.

## A.7 Drude-ionized oscillator

The “Drude-ionized” oscillator is a modified Drude oscillator with an energy dependence of the scattering time  $\tau$  which approximates the one predicted when the carrier scattering is caused by ionized impurities. In that case  $\tau$  is constant from zero frequency (DC case) up to about  $0.75 \cdot \omega_N$  (where  $\omega_N^2 = (q^2 N)/(m^* \epsilon_0)$ ) while for higher frequencies  $\tau$  increases as  $\omega^{3/2}$  [19–21]. The broadening parameter  $D(E)$  in this oscillator is therefore a function of the energy: it is equal to the input value  $D$  for energies lower than the transition energy  $E_{tr} = 0.75(2C/\pi)^{1/2}$  while for higher energies it is given by  $D(E) = D(E_{tr}/E)^{3/2}$ .

If this oscillator is used to fit the optical constants of TCO instead of the simple Drude oscillator, the main difference is a reduced absorption in the energy region between  $E_g$  and  $E_{tr}$ .

## A.8 Direct and Indirect gap oscillators

The oscillators introduced up to now are unsuitable to describe the optical constants of systems with a continuous distribution of density of states such as semiconductors.

As a matter of fact the semiconductors theories reported in textbooks [22] usually derive  $\epsilon_2 = \chi_2$  only and exclusively at energies near the fundamental gap. Furthermore the calculation is made by hypothesizing that the excited states have infinite lifetime, i.e. that every transition between two states may take place only by absorbing photons which energy is exactly equal to the difference of their energetic levels; the real part  $\epsilon_1$  is not explicitly calculated, but it can be obtained by means of the Kramers-Kronig relations (Eq. 4). Since the Kramers-Kronig integrals have to be numerically computed (except for particular cases) that approach could be somewhat slow for best-fit procedures.

In the previous version of kSEMAWc analytical expressions for both  $\chi_1$  and  $\chi_2$ , satisfying the Kramers-Kronig relations and having a clear physical interpretation, were exclusively used. In this version of kSEMAWc we have also added some oscillators computed using Kramers-Kronig integrals to allow the description of exponential (Urbach) tails at the absorption band edges of semiconductors.

The analytical expressions are obtained by performing the convolution between a suitable  $\chi_2^{inf}$  calculated for infinite lifetime and the normalized complex  $\tilde{\chi}_{qo}$  describing the response of a quantum oscillator:

$$\tilde{\chi}(E) = \int \chi_2^{inf}(E_r) \tilde{\chi}_{qo}(E_r - E) dE_r \quad (6)$$

The function  $\tilde{\chi}_{qo}$  is given by the expression given before normalized so that the integral of its imaginary part is equal to 1:

$$\tilde{\chi}_{qo}(E, E_r) = \frac{1}{\pi D} \left[ \frac{(E_r - E)/D}{1 + [(E_r - E)/D]^2} - i \frac{1}{1 + [(E_r - E)/D]^2} \right] \quad (7)$$

where  $E_r$  is the resonance energy.

The result of the convolution can be expressed as analytical functions in a few simple but interesting cases discussed below.

In general  $\chi_2^{inf}$  can be expressed as the product of the joint density of states  $\rho(E)$  and a transition intensity  $I(E)$  [23]:

$$\chi_2^{inf}(E) = I(E)\rho(E) \quad (8)$$

$I(E)$  contains the squared modulus of the matrix element of the electron-photon interaction Hamiltonian between the initial and final states. In the dipole approximation  $I(E)$  is proportional to the squared modulus of the position operator ( $|\langle r \rangle|^2$ ) but it can be written in an equivalent way also by using the momentum operator. A relation between the matrix elements of these two operators can be obtained by using commutator relations:

$$|\langle r \rangle|^2 = |\langle p \rangle|^2 \left( \frac{\hbar}{mE} \right)^2 \quad (9)$$

The energy dependence of the matrix elements and consequently of  $I(E)$  cannot be easily predicted and therefore  $I(E)$  is assumed to be a constant if  $|\langle r \rangle|^2$  is supposed to be independent of energy while it is assumed to be proportional to  $1/E^2$  if  $|\langle p \rangle|^2$  is supposed to be independent of energy. The constant  $|\langle p \rangle|^2$  assumption was used by Tauc et al. [24]

in the interpretation of the optical absorption of amorphous semiconductors leading to the well known "Tauc plot" method to derive the optical gap. The constant  $|\langle r \rangle|^2$  assumption was later proposed by Cody [25] again for the amorphous semiconductor case. These two alternatives can be used for crystalline materials also. For example in crystalline GaAs the energy dependence of the optical absorption above the bandgap is better described by the constant position matrix element [23] instead of by the more commonly hypothesized constant momentum matrix element.

For a crystalline semiconductor with direct allowed transitions between two parabolic bands separated by an energy gap  $E_0$ ,  $\rho(E)$  can be written as [22]:

$$\rho(E) = C_r(E - E_0)^{1/2} \quad (10)$$

This monotonically increasing expression for  $\rho(E)$  is obviously valid only for energies slightly larger than the gap. For higher energy values  $\rho(E)$  can show a rather complex behavior but it also has a high energy limit determined by the extension of the valence and conduction bands. At the gap energy ( $E_0$ ) and at this high energy limit ( $E_3 = E_0 + W$ ) the  $\rho(E)$  has two "critical points" called  $M0$  and  $M3$  where it goes to zero following a square root behavior [22].

The simplest expression valid for every energy which has the correct square root behaviour near  $E_0$  and  $E_3$  is:

$$\rho(E) = C_r \sqrt{(E - E_0)(E_3 - E)} \quad (11)$$

By using this expression and the "Cody's approximation" the  $\chi_2^{inf}$  also has the same form:

$$\chi_{2-dir-Cody}^{inf}(E) = \frac{C}{K_{Cd}} \sqrt{(E - E_0)(E_3 - E)} \quad (12)$$

Equation 12 can be considered as an acceptable approximation for  $\chi_2^{inf}(E)$  in the case of a direct gap material with position matrix element independent of energy and with infinite lifetime (see Fig. 13 a)).

The normalization constant  $K_{Cd}$  is given by:

$$K_{Cd} = \int_{E_0}^{E_0+W} E \sqrt{(E - E_0)(E_3 - E)} dE = \frac{\pi}{16} W^2 (2E_0 + W)$$

On the other hand in Tauc's approximation, the momentum matrix element is considered as independent of energy; therefore as previously discussed an additional factor  $1/E^2$  has to be inserted in the formula (see Fig. 13 b)):

$$\chi_{2-dir-Tauc}^{inf}(E) = \frac{C}{K_{Td}} \frac{\sqrt{(E - E_0)(E_3 - E)}}{E^2} \quad (13)$$

The normalization constant  $K_{Td}$  is given by:

$$K_{Td} = \int_{E_0}^{E_0+W} E \frac{\sqrt{(E - E_0)(E_3 - E)}}{E^2} dE = \frac{\pi}{2} (2E_0 + W - 2\sqrt{E_0(E_0 + W)})$$

Other types of critical points do exist in the  $\rho(E)$  [22] and two of them ( $M1$  and  $M2$ ) are discussed later on.

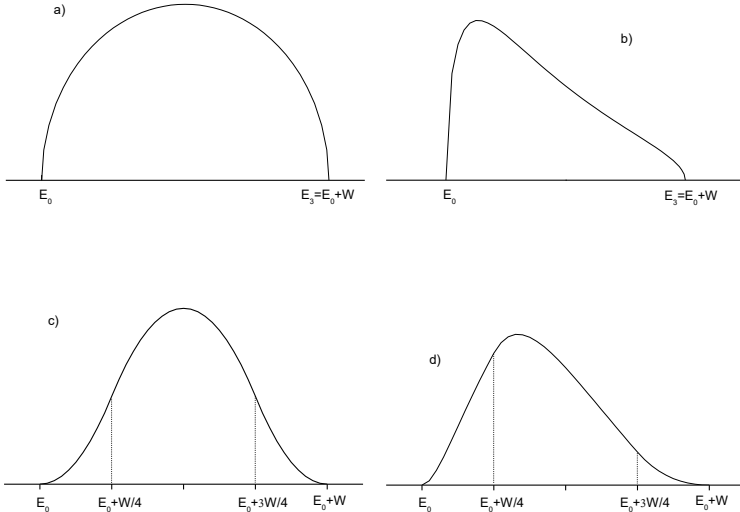


Figure 13:  $\chi_2^{inf}$  for infinite lifetime semiconductor and: a) direct gap under Cody's approximation b) direct gap under Tauc's approximation, c) indirect gap under Cody's approximation d) indirect gap under Tauc's approximation

In the two previous cases we considered direct transitions i.e. transitions where the excitation takes place with the absorption of a single photon. In this case the crystalline momentum of the electron excited in the conduction band must be practically equal to the momentum of the electron in the valence band.

Different formulas must be used for materials where the fundamental gap is due to indirect transitions: in this case the excitation process includes the absorption or the emission of a phonon necessary to allow transitions between electronic states with different crystalline momentum. The absorption/emission of phonon remove the momentum conservation constraint and therefore for indirect transitions  $\rho(E)$  is proportional to the convolution of the density of states of the two bands. In amorphous semiconductors also the momentum conservation is not required because the disorder destroy translational symmetry and momentum is no more a good quantum number. It follows that oscillators for indirect transitions in crystalline semiconductors can be used to fit the optical constants of amorphous semiconductors too.

Unfortunately the convolution integral of two finite valence and conduction bands of the form given by Eq. 11 has no analytical expression. On the other hand it is well known that the convolution between two square root densities of states gives a function which increases parabolically above the gap. Therefore an empirical approximated expression can be obtained by joining two parabolic edges with a parabolic maximum, getting in the Cody's approximation (see Fig. 13 c):

$$\chi_{2-ind-Cody}^{inf}(E) = \frac{16C}{K_{Ci}W^2}(E - E_0)^2 \quad \text{if } E_0 < E < E_0 + W/4 \quad (14)$$

$$\chi_{2-ind-Cody}^{inf}(E) = \frac{C}{K_{Ci}} \left\{ 2 - \frac{16}{W^2} [E - (E_0 + W/2)]^2 \right\} \quad \text{if } E_0 + \frac{W}{4} < E < E_0 + \frac{3W}{4} \quad (15)$$

$$\chi_{2-ind-Cody}^{inf}(E) = \frac{16C}{K_{Ci}W^2} [E - (E_0 + W)]^2 \quad \text{if } E_0 + \frac{3W}{4} < E < E_0 + W \quad (16)$$

where  $E_0$  is the gap energy and  $W$  is the absorption band width. The normalization constant  $K_{Ci}$  is given by:

$$K_{Ci} = E_0 W + \frac{W^2}{2} \quad (17)$$

In the Tauc's approximation the expressions are obviously (see Fig. 13 d):

$$\chi_{2-ind-Tauc}^{inf}(E) = \frac{16C}{K_{Ti}W^2E^2}(E - E_0)^2 \quad \text{if } E_0 < E < E_0 + W/4 \quad (18)$$

$$\chi_{2-ind-Tauc}^{inf}(E) = \frac{C}{K_{Ti}E^2} \left\{ 2 - \frac{16}{W^2} \left[ E - (E_0 + \frac{W}{2}) \right]^2 \right\} \quad \text{if } E_0 + \frac{W}{4} < E < E_0 + \frac{3W}{4} \quad (19)$$

$$\chi_{2-ind-Tauc}^{inf}(E) = \frac{16C}{K_{Ti}W^2E^2} [E - (E_0 + W)]^2 \quad \text{if } E_0 + \frac{3W}{4} < E < E_0 + W \quad (20)$$

The normalization constant  $K_{Ti}$  is given by:

$$K_{Ti} = f(E_0/W) \quad (21)$$

where

$$f(r) = 2 \left[ 8r^2 \ln \left( \frac{4r+1}{4r} \right) + 8(r+1)^2 \ln \left( \frac{4r+4}{4r+3} \right) - (1+8(r^2+r)) \ln \left( \frac{4r+3}{4r+1} \right) \right] \quad (22)$$

To connect these expressions to the usual plots used to extract the semiconductor bandgap from the absorption coefficient spectrum it is enough to remember that:

$$\alpha = \frac{\omega\epsilon_2}{nc}$$

The ensuing plots are listed in Table III

Gap type	Absorption coefficient	Plot
Tauc direct	$\alpha \propto (E - E_g)^{1/2}/E$	$(\alpha E)^2 \propto (E - E_g)$
Tauc indirect	$\alpha \propto (E - E_g)^2/E$	$(\alpha E)^{1/2} \propto (E - E_g)$
Cody direct	$\alpha \propto (E - E_g)^{1/2}E$	$(\alpha/E)^2 \propto (E - E_g)$
Cody indirect	$\alpha \propto (E - E_g)^2E$	$(\alpha/E)^{1/2} \propto (E - E_g)$

Table III: Plot to find  $E_g$  for different gap types

The complex expressions obtained by performing the convolution between the  $\chi_2^{inf}$  and the normalized complex  $\tilde{\chi}_{qo}$  in the four cases are:

**Direct gap Cody:**

$$\begin{aligned} \chi_{1-dir-Cody}(E) &= \frac{CD}{2K_{Cd}} \left\{ a + b - 2(a^2 + 1)^{1/4}(b^2 + 1)^{1/4} \right. \\ &\times \cos \left[ \frac{1}{2} \arctan \left( \frac{1}{a} \right) + \frac{1}{2} \arctan \left( \frac{1}{b} \right) \right] \left. \right\} = \frac{CD}{2K_{Cd}} \left[ a + b - 2\Re \left( \sqrt{a+i}\sqrt{b+i} \right) \right] \quad (23) \end{aligned}$$

$$\begin{aligned} \chi_{2-dir-Cody}(E) &= -\frac{CD}{K_{Cd}} \left\{ 1 + (a^2 + 1)^{1/4}(b^2 + 1)^{1/4} \right. \\ &\times \sin \left[ \frac{1}{2} \arctan \left( \frac{1}{a} \right) + \frac{1}{2} \arctan \left( \frac{1}{b} \right) \right] \left. \right\} = -\frac{CD}{K_{Cd}} \left[ 1 - \Im(\sqrt{a+i}\sqrt{b+i}) \right] \quad (24) \end{aligned}$$

where  $a = \frac{E_0-E}{D}$  and  $b = \frac{E_3-E}{D}$ .

**Direct gap Tauc**

$$\begin{aligned} \chi_{1-dir-Tauc}(E) &= \frac{C}{2DK_{Td}} \Re \left\{ \frac{1}{2(D-iE)} \left( 2iD + 2E - 2\sqrt{E_0E_3} \right. \right. \\ &\left. \left. - (i-1)\sqrt{2}\sqrt{D-i(E-E_0)}\sqrt{-iD-E+E_3} \right) \right. \\ &+ \frac{1}{2(D+iE)} \left( -2iD + 2E - 2\sqrt{E_0E_3} + (i+1)\sqrt{2}\sqrt{D+i(E-E_0)}\sqrt{iD-E+E_3} \right) \\ &\quad + E(D-iE)^2 \sqrt{D+i(E-E_0)} \sqrt{D+i(E-E_3)} / (D^2+E^2)^2 \\ &\quad + E(D+iE)^2 \sqrt{D-i(E-E_0)} \sqrt{D-i(E-E_3)} / (D^2+E^2)^2 \\ &\left. - ED \left( D^2(E_0+E_3) + E(-4E_0E_3 + E(E_0+E_3)) \right) / \left( (D^2+E^2)^2 \sqrt{E_0E_3} \right) \right\} \quad (25) \end{aligned}$$

$$\begin{aligned} \chi_{2-dir-Tauc}(E) &= \frac{CD}{K_{Td}} \\ &\times \Re \left\{ - \left[ (D-iE)^2 \sqrt{D+i(E-E_0)} \sqrt{D+i(E-E_3)} \right] / \left( 2D (D^2+E^2)^2 \right) \right. \\ &\quad - \left[ (D+iE)^2 \sqrt{D-i(E-E_3)} \sqrt{D-i(E-E_0)} \right] / \left( 2D (D^2+E^2)^2 \right) \\ &\quad \left. + D [D^2(E_0+E_3) + E(-4E_0E_3 + E(E_0+E_3))] / \left( 2D (D^2+E^2)^2 \sqrt{E_0E_3} \right) \right\} \quad (26) \end{aligned}$$

**Indirect gap-Cody**

$$\begin{aligned} \chi_{1-ind-Cody}(E) &= \frac{C}{K_{Ci}} \left\{ 2IC_{Re}^{Cody}(E, E_0 + 3W/4) - 2IC_{Re}^{Cody}(E, E_0 + W/4) \right. \\ &\quad + 16/W^2 \left[ I2_{Re}^{Cody}(E, E_0, E_0 + W/4) - I2_{Re}^{Cody}(E, E_0, E_0) \right. \\ &\quad - I2_{Re}^{Cody}(E, E_0 + W/2, E_0 + 3W/4) + I2_{Re}^{Cody}(E, E_0 + W/2, E_0 + W/4) \\ &\quad \left. \left. + I2_{Re}^{Cody}(E, E_0 + W, E_0 + W) - I2_{Re}^{Cody}(E, E_0 + W, E_0 + 3W/4) \right] \right\} \quad (27) \end{aligned}$$

where:

$$IC_{Re}^{Cody}(E, E_r) = \frac{1}{\pi D} \int \frac{[(E_r - E)/D] dE_r}{1 + [(E_r - E)/D]^2} = \frac{1}{2\pi} \ln [D^2 + (E - E_r)^2] \quad (28)$$

$$\begin{aligned} I2_{Re}^{Cody}(E, E_0, E_r) &= \frac{1}{\pi D} \int \frac{(E_r - E_0)^2 [(E_r - E)/D] dE_r}{1 + [(E_r - E)/D]^2} \\ &= \frac{1}{2\pi} \left\{ (E_r - E)(3E - 4E_0 + E_r) + 4D(E - E_0) \arctan \left( \frac{E - E_r}{D} \right) \right. \\ &\quad \left. + [(E - E_0)^2 - D^2] \ln [D^2 + (E - E_r)^2] \right\} \quad (29) \end{aligned}$$

$$\begin{aligned} \chi_{2-ind-Cody}(E) &= \frac{C}{K_{Ci}} \left\{ 2IC_{Im}^{Cody}(E, E_0 + 3W/4) - 2IC_{Im}^{Cody}(E, E_0 + W/4) \right. \\ &\quad + 16/W^2 \left[ I2_{Im}^{Cody}(E, E_0, E_0 + W/4) - I2_{Im}^{Cody}(E, E_0, E_0) \right. \\ &\quad - I2_{Im}^{Cody}(E, E_0 + W/2, E_0 + 3W/4) + I2_{Im}^{Cody}(E, E_0 + W/2, E_0 + W/4) \\ &\quad \left. \left. + I2_{Im}^{Cody}(E, E_0 + W, E_0 + W) - I2_{Im}^{Cody}(E, E_0 + W, E_0 + 3W/4) \right] \right\} \quad (30) \end{aligned}$$

where:

$$IC_{Im}^{Cody}(E, E_r) = \frac{1}{\pi D} \int \frac{dE_r}{1 + [(E_r - E)/D]^2} = -\frac{1}{\pi} \arctan \left( \frac{E - E_r}{D} \right) \quad (31)$$

$$\begin{aligned} I2_{Im}^{Cody}(E, E_0, E_r) &= \frac{1}{\pi D} \int \frac{(E_r - E_0)^2 dE_r}{1 + [(E_r - E)/D]^2} \\ &= \frac{1}{\pi} \left( [D^2 + (E - E_0)^2] \arctan \left( \frac{E - E_r}{D} \right) \right. \\ &\quad \left. + D \{ E_r - E + (E - E_0) \ln [D^2 + (E - E_r)^2] \} \right) \quad (32) \end{aligned}$$

### Indirect gap-Tauc

$$\begin{aligned} \chi_{1-ind-Tauc}(E) &= \frac{C}{K_{Ti}} \left\{ 2IC_{Re}^{Tauc}(E, E_0 + 3W/4) - 2IC_{Re}^{Tauc}(E, E_0 + W/4) \right. \\ &\quad + 16/W^2 \left[ +I2_{Re}^{Tauc}(E, E_0, E_0 + W/4) - I2_{Re}^{Tauc}(E, E_0, E_0) \right. \\ &\quad - I2_{Re}^{Tauc}(E, E_0 + W/2, E_0 + 3W/4) + I2_{Re}^{Tauc}(E, E_0 + W/2, E_0 + W/4) \\ &\quad \left. \left. + I2_{Re}^{Tauc}(E, E_0 + W, E_0 + W) - I2_{Re}^{Tauc}(E, E_0 + W, E_0 + 3W/4) \right] \right\} \quad (33) \end{aligned}$$

where:

$$\begin{aligned}
IC_{Re}^{Tauc}(E, E_r) &= \frac{1}{\pi D} \int \frac{[(E_r - E)/D] dE_r}{E_r^2 [1 + [(E_r - E)/D]^2]} \\
&= \frac{1}{2\pi(D^2 + E^2)^2} \left\{ -4DE \arctan \left( \frac{E - E_r}{D} \right) \right. \\
&\quad \left. + \frac{2E(D^2 + E^2)}{E_r} + (E^2 - D^2) \ln \left( \frac{D^2 + (E - E_r)^2}{E_r^2} \right) \right\} \quad (34)
\end{aligned}$$

$$\begin{aligned}
I2_{Re}^{Tauc}(E, E_0, E_r) &= \frac{1}{\pi D} \int \frac{(E_r - E_0)^2 [(E_r - E)/D] dE_r}{E_r^2 [1 + [(E_r - E)/D]^2]} \\
&= \frac{1}{2\pi(D^2 + E^2)^2} \left\{ 4DE_0(D^2 + E^2 - EE_0) \arctan \left( \frac{E - E_r}{D} \right) \right. \\
&\quad + [D^4 + E^2(E - E_0)^2 + D^2(2E^2 - 2EE_0 - E_0^2)] \ln(D^2 + (E - E_r)^2) \\
&\quad \left. + 2E_0 \left[ \frac{E(D^2 + E^2)E_0}{E_r} + (E^2(2E - E_0) + D^2(2E + E_0)) \ln(E_r) \right] \right\} \quad (35)
\end{aligned}$$

$$\begin{aligned}
\chi_{2-ind-Tauc}(E) &= \frac{C}{K_{Ti}} \left\{ 2IC_{Im}^{Tauc}(E, E_0 + 3W/4) - 2IC_{Im}^{Tauc}(E, E_0 + W/4) \right. \\
&\quad + 16/W^2 [ +I2_{Im}^{Tauc}(E, E_0, E_0 + W/4) - I2_{Im}^{Tauc}(E, E_0, E_0) \\
&\quad - I2_{Im}^{Tauc}(E, E_0 + W/2, E_0 + 3W/4) + I2_{Im}^{Tauc}(E, E_0 + W/2, E_0 + W/4) \\
&\quad \left. + I2_{Im}^{Tauc}(E, E_0 + W, E_0 + W) - I2_{Im}^{Tauc}(E, E_0 + W, E_0 + 3W/4) \right\} \quad (36)
\end{aligned}$$

where:

$$\begin{aligned}
IC_{Im}^{Tauc}(E, E_r) &= \frac{1}{\pi D} \int \frac{dE_r}{E_r^2 [1 + [(E_r - E)/D]^2]} \\
&= -\frac{1}{\pi(D^2 + E^2)^2} \left\{ (E^2 - D^2) \arctan \left( \frac{E - E_r}{D} \right) \right. \\
&\quad \left. + D \left[ \frac{(D^2 + E^2)}{E_r} + E \ln \left( \frac{D^2 + (E - E_r)^2}{E_r^2} \right) \right] \right\} \quad (37)
\end{aligned}$$

$$\begin{aligned}
I2_{Im}^{Tauc}(E, E_0, E_r) &= \frac{1}{\pi D} \int \frac{(E_r - E_0)^2 dE_r}{E_r^2 [1 + [(E_r - E)/D]^2]} \\
&= -\frac{1}{\pi(D^2 + E^2)^2} \left\{ [D^4 + E^2(E - E_0)^2 + D^2(2E^2 - 2EE_0 - E_0^2)] \arctan \left( \frac{E - E_r}{D} \right) \right. \\
&\quad \left. + DE_0 \left[ \frac{(D^2 + E^2)E_0}{E_r} + (D^2 + E^2 - EE_0) \ln \left( \frac{E_r^2}{D^2 + (E - E_r)^2} \right) \right] \right\} \quad (38)
\end{aligned}$$

## A.9 Oscillators with an Urbach tail at the band edges

The absorption bands of the just described four oscillators, for direct and indirect gap, show wide Lorentzian tails which cause a not-negligible absorption also far from the absorption band (see the black line in Fig. 14 referring to the direct gap Cody oscillator). On the other hand quite often the semiconductor absorption band edge decreases in a sharper way, well described by the so-called exponential Urbach tail. To include such a behavior, since version 2.0, kSEMAWc includes four more oscillators. The  $\chi_2(E)$  of these new oscillators are obtained by adding two exponential tails ( $\chi_2(E) \propto \exp(\pm E/D)$ ) at the absorption band sides of the four  $\chi_2^{inf}(E)$  shown in Fig. 13; the junction points are chosen so that the global function and its first derivative are continuous. The corresponding  $\chi_1(E)$  are then computed by the numerical integration of the Kramers-Kronig relationship (Eq. 4). Figure 14 shows the application of the above-described procedure to the case of the direct Cody absorption band  $\chi_2^{inf}(E)$  (blue curve), where the red curve represents the  $\chi_2(E)$  of the new oscillator with tails modeled according to Urbach's theory.

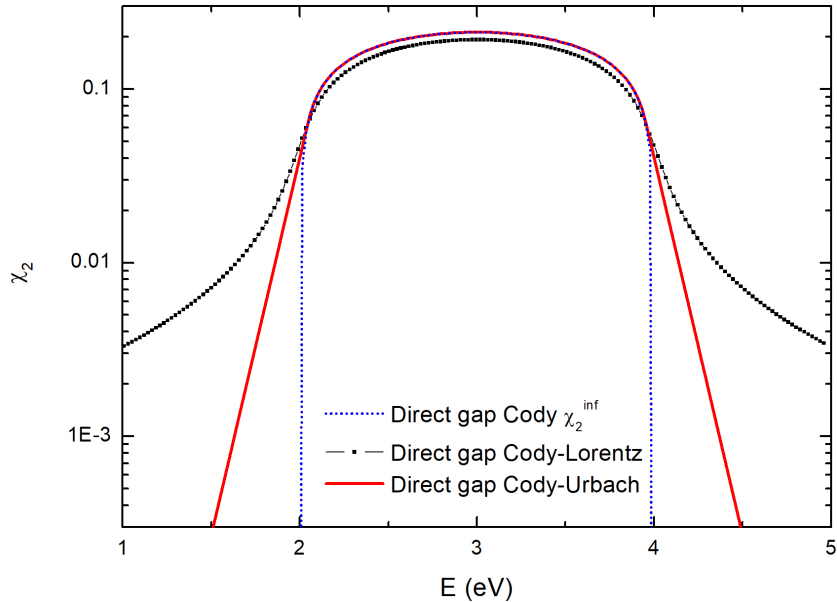


Figure 14: the blue curve shows  $\chi_2^{inf}(E)$  for direct gap under Cody's approximation. The black curve represents  $\chi_2(E)$  computed by the convolution with a quantum oscillator. The red curve is obtained from  $\chi_2^{inf}(E)$  by adding the Urbach tails. The parameters are:  $C=1$ ,  $E_0 = 2$  eV,  $W = 2$  eV,  $D = 0.1$  eV. The parameter  $D$  corresponds to the quantum oscillator line width in one case and to the characteristic energy of the Urbach tail ( $\chi_2(E) \propto \exp(\pm E/D)$ ) in the other one.

## A.10 Direct Gap Tauc-Exciton oscillator

For many interesting materials the absorption edge is substantially influenced by the possibility to form excitons upon photon absorption. The exciton is an excited state with an energy lower than that of the free carriers due to the electron and hole Coulomb attraction. Similarly to atoms, the excitons have both a discrete spectrum due to bound states but also the unbound states, which form a continuous density of states, are different from the usual free particle states. Obviously for energies much larger than the exciton binding energy the two densities of states converge. The peaks due to the discrete spectrum are visible only if the exciton binding energy  $W$  is large enough and if the line broadening  $D$  is small enough. A theory which describes the effects of excitons was developed in 1957 by Elliott [26]. The oscillator included in kSEMAWc is based on an improved version of the Elliott's theory presented by Tanguy in 1995 [27] which gives a very compact expression for the susceptibility of a semiconductor with a direct gap in the Tauc approximation taking into account the excitons and a Lorentzian broadening of the states :

$$\tilde{\chi}(E) = \frac{C\sqrt{W}}{(E + iD)^2} [g_a(\xi(E + iD)) + g_a(\xi(-E - iD)) - 2g_a(\xi(0))] \\ g_a(\xi) = 2 \ln \xi - 2\pi \cot(\pi\xi) - 2\psi(\xi) - 1/\xi \\ \xi(z) = \sqrt{\frac{W}{E_0 - z}}$$

where  $\psi(z) = d \ln \Gamma(z)/dz$  is the complex digamma function,  $D$  is the width of the Lorentzian broadening function,  $E_0$  is the energy gap and  $W$  is the exciton binding energy. For this oscillator the intensity parameter  $C$  cannot be normalized as in the other cases since the function  $\tilde{\chi}(E)E$  decays as  $1/\sqrt{E}$  for large values of  $E$  and therefore the sum rule integral diverges.

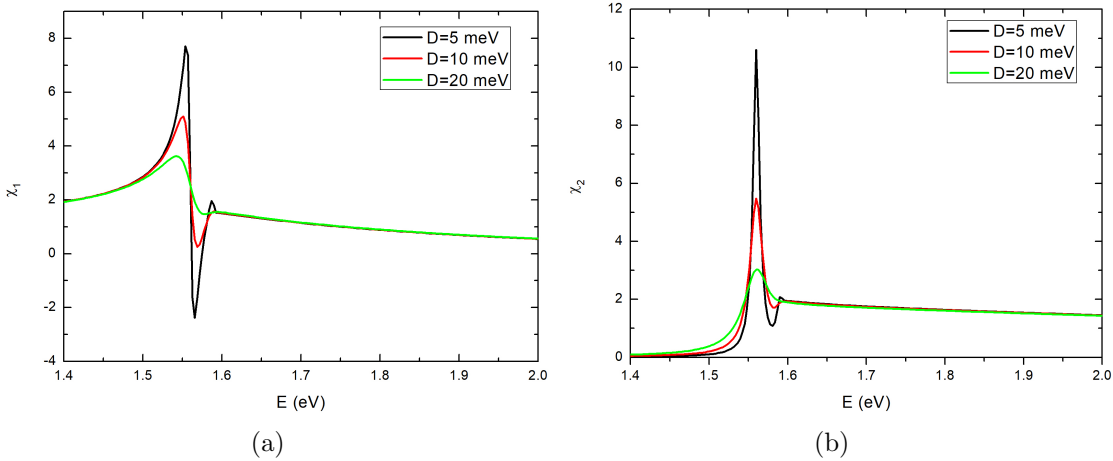


Figure 15: Plot of  $\chi_1$  and  $\chi_2$  for a Direct Gap Tauc-Exciton oscillators with  $C=4$ ,  $E_0 = 1.6$  eV,  $W=40$  meV and for three different values of the broadening parameter  $D$ : 5,10,20 meV.

It is interesting to note that the absorption in the energy region near the gap increases significantly with increasing exciton binding energy (thank to the so-called Sommerfeld enhancement factor) as shown in Fig. 16

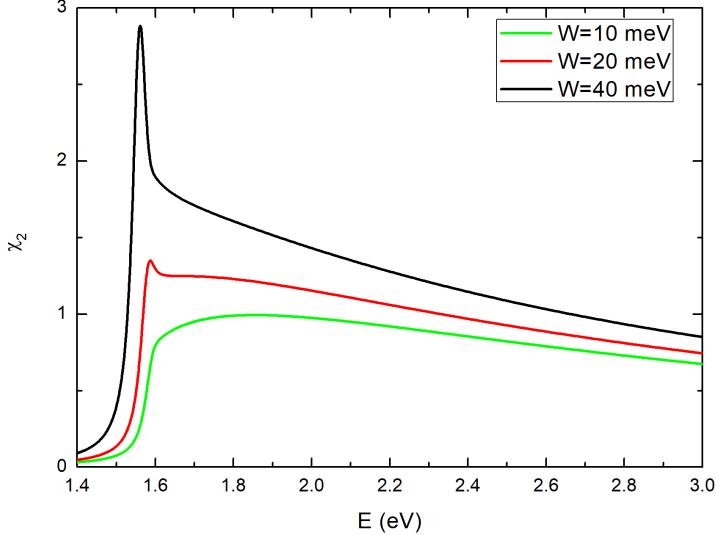


Figure 16: Behaviour of  $\chi_2$  for a Direct Gap Tauc-Exciton oscillators with  $C=4$ ,  $E_0 = 1.6$  eV,  $D=20$  meV and for three different values of the exciton binding energy  $W$ : 10, 20, 40 meV.

According to some authors the excitonic effects, being not local, lead to a break down of the sum rule expressed by Eq. 5 and therefore they cannot be interpreted as a simple redistribution of oscillators [28].

### A.11 3D M1-M2 critical points oscillator

As pointed out earlier, several other types of critical points do exist in addition to M0 and M3. In version 2.1 we have included two oscillators for the modeling of three dimensional M1-M2 critical points. These oscillators were built starting from the density of states for a simple cubic lattice in the Tight-Binding s-level nearest-neighbor approximation with an overlap integral equal to  $D$ . The resulting  $\rho_{s.c.}(E)$  has been calculated numerically [29] and it has a width  $W = E_3 - E_0 = 6D$  and shows, in addition to the two critical point at  $E_0$  and  $E_3$ , other two critical point called 3D M1 and M2 where the slope becomes infinite, again with a square root behavior. The numerically calculated  $\rho_{s.c.}(E)$  in a simple cubic material can be approximated by an analytical expression given by [30]:

$$\rho_{s.c.}(E) = A\sqrt{(E - E_0)(E_3 - E)} + B \left[ \sqrt{2D} - \Theta(|E - \bar{E}| - D)\sqrt{|E - \bar{E}| - D} \right] + C(E - E_0)(E - E_3) \quad (39)$$

where  $\bar{E} = (E_3 + E_0)/2$ ,  $A=0.030491$ ,  $B=0.213231$  and  $C=0.0121189$ . A plot of this function is reported in Fig. 17

The first term in Eq. 39 corresponds to the density of states used in the direct gap oscillators. To get more flexibility in the fitting procedure we preferred therefore to use those oscillators to model the M0-M3 critical points and to set up a separate oscillators for M1-M2 critical points. To obtain an expression valid for arbitrary values of  $D$  the second term is slightly modified and the values of the ratio  $B/C$  is chosen so that the derivative of function  $\rho_{M1M2}(E)$  is zero at both  $E_0$  and  $E_3$ :

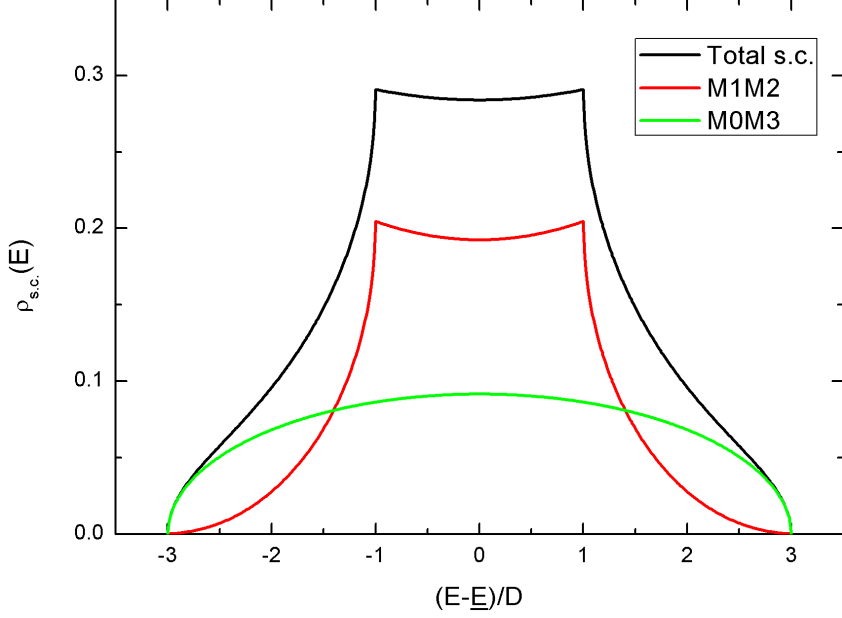


Figure 17: Density of states  $\rho_{s.c.}(E)$  for a simple cubic lattice in the Tight-Binding s-level nearest-neighbor approximation with an overlap integral equal to  $D$  (black curve). The separation of the density of states in two contribution from M0-M3 (green curve) and M1-M2 (red curve) is also shown.

$$\begin{aligned} \rho_{M1M2}(E) &= B \left[ \sqrt{\frac{W}{2} - D} - \Theta(|E - \bar{E}| - D) \sqrt{|E - \bar{E}| - D} \right] + C(E - E_0)(E - E_3) \\ B &= 2C(E_3 - E_0) \sqrt{\frac{E_3 - E_0}{2} - D} = K_1 C \end{aligned}$$

By using this expression we obtain in the Cody's approximation :

$$\chi_{2-CM12}(E) = \frac{C}{K_{CM12}} \left\{ K_1 \left[ \sqrt{\frac{W}{2} - D} - \Theta(|E - \bar{E}| - D) \sqrt{|E - \bar{E}| - D} \right] + (E - E_0)(E - E_3) \right\} \quad (40)$$

where the normalization constant  $K_{CM12}$  is given by:

$$\begin{aligned} K_{CM12} &= \frac{(E_3^2 - E_0^2)}{6} \left[ E_0 E_3 - \frac{(E_3^2 + E_0^2)}{2} \right] + \frac{K_1}{2} \sqrt{\frac{W}{2} - D} (E_3^2 - E_0^2) \\ &\quad - \frac{2K_1}{15} \sqrt{\bar{E} - D - E_0} [2(\bar{E} - D)^2 - 3E_0^2 + E_0(\bar{E} - D)] \\ &\quad - \frac{2K_1}{15} \sqrt{-\bar{E} - D + E_3} [-2(\bar{E} + D)^2 + 3E_3^2 - E_3(\bar{E} + D)] \quad (41) \end{aligned}$$

In the Tauc's approximation we have instead:

$$\chi_{2-TM12}(E) = \frac{CE^{-2}}{K_{TM12}} \left\{ K_1 \left[ \sqrt{\frac{W}{2} - D} - \Theta(|E - \bar{E}| - D) \sqrt{|E - \bar{E}| - D} \right] + (E - E_0)(E - E_3) \right\} \quad (42)$$

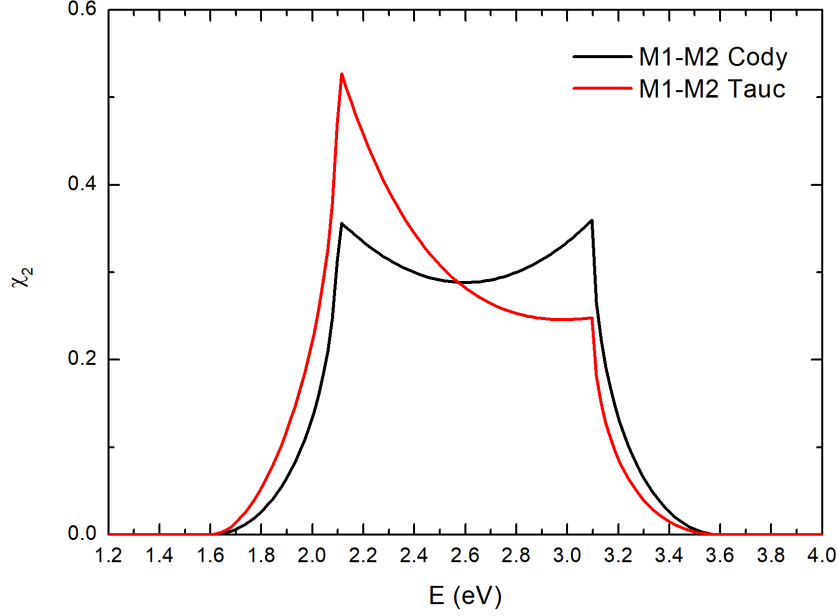


Figure 18: Plot of  $\chi_2$  for a M1-M2 oscillators with  $C=1 \text{ eV}^2$ ,  $E_0 = 1.6 \text{ eV}$ ,  $W = 2\text{eV}$  and  $D=0.5 \text{ eV}$  using the Cody (black curve) and Tauc (red curve) approximations.

where the normalization constant  $K_{TM12}$  is given by:

$$\begin{aligned}
 K_{TM12} = & -\frac{(E_3^2 - E_0^2)}{2} + \log\left(\frac{E_3}{E_0}\right) \left[ E_0 E_3 + K_1 \sqrt{\frac{W}{2} - D} \right] + \\
 & + 2K_1 \left\{ \sqrt{E - D - E_0} - \sqrt{E - D} \left[ \log\left(\frac{\sqrt{E - D} + \sqrt{E - D - E_0}}{\sqrt{E_0}}\right) \right] \right\} \\
 & - 2K_1 \left\{ \sqrt{E_3 - E - D} + \sqrt{E + D} \left[ \arcsin\left(\sqrt{\frac{E + D}{E_3}}\right) - \frac{\pi}{2} \right] \right\} \quad (43)
 \end{aligned}$$

## B Some useful rules of good practice

During my experience developed over thirty years, I have often observed that neophytes tend to underestimate the difficulties associated with spectrophotometric measurements; these difficulties become even greater when one needs the absolute values of the measurement, as requested by kSEMAWc.

Without any claim of exhaustiveness, I list below some rules that users should take care to fulfill in order to avoid the most common mistakes.

### B.1 $n,k$ of the substrate

The most common error in characterizing thin film devices is to neglect the preliminary characterization of the substrate. As a matter of fact, although for a given type of material the real part of the refractive index is fairly constant over different specimens, and well compatible with the values reported in literature, the same cannot be said for the extinction coefficient: in the nearness of the absorption edges, such as the UV transmittance cutoff for glass and quartz, the user should not be surprised to find differences much greater than the measurement error, even among substrates belonging to the same batch! Thus if one intends to analyze a series of samples, the preliminary check about the homogeneity of the available substrates and, if necessary, the selection of a group with same features, are mandatory. In order to properly characterize thin film specimens, the loading in the *Valin* TAB of the right  $nk$ -file is essential, otherwise the found solutions will be subject to more or less evident artifacts.

### B.2 Reflectance reference

Unless reflectance is measured by means of an absolute accessory, a reference specimen is required. A very common error is to measure the hemispherical reflectance of a sample with good specular characteristics by using a diffusive reference, like the cover of the port supplied with the integrating sphere. This will lead to artifacts induced by the dependence, albeit weak, of the response of an integrating sphere from the emission angle, with respect to the optical axis, of the transmitted/reflected rays.

In the case of relative specular reflectance accessories, a frequent error is to overlook the dependence of the response on the distance between the most reflective surface and the reference plane on which the sample lays (for example three tips). As an example, *first-face* mirrors (i.e. with reflective treatment on the *front face*) should not be measured using *second-face* reference mirrors; in this case the error will be larger for reference mirrors with thicker substrates.

Consequently, the following golden rule must be respected: **always use a reference sample as similar as possible to the sample to be characterized: specular for specular, diffusive for diffusive, etc ..**

When a certified sample suitable for own needs is purchased, a secondary reference sample, even homemade, should be obtained and used in everyday measurements.

If mirrors/specimens are placed on a reference plane (i.e. the exit port of the integrating sphere), it is strongly recommended to make a frame spacer in which to insert the mirror, in order to avoid the direct contact between reflective and reference surfaces.

### B.3 Prismatic sample

A sample with not perfectly parallel faces, like a prism, induces the deviation of the beam passing through it; in reflection instead it will give rise to two diverging beams.

The prismatic angle of the sample can be quantitatively assessed using a laser beam; otherwise the user should simply observe by eye the image reflected from the sample surface, of an object with well-defined edges, such as a neon lamp.

Except for the case of integrating spheres, the transmitted (reflected) beam(s) will impact the sensitive area of the detector in different sites (with respect to the calibration/baseline measurement); sometimes part of the beam(s) will fall out the detector; all this will significantly affect the measured value. In order to evaluate the entity of this problem, the user should observe the eventual variation of the signal obtained by rotating the sample around the optical axis of the instrument.

There are two solutions to this problem: i) use an integrating sphere; ii) use an integrating sphere just like a sensor in specular/direct measurements. The last solution requires that the spectrophotometer can be simultaneously equipped with an integrating sphere and a specular reflectance accessory; as for the transmittance, it will be enough to place the sample at an appropriate distance from the entry port of the integrating sphere.

### B.4 Masks for small area samples

Samples made in research laboratories often offer a useful surface which is smaller than the section of the measurement beam. Unless the focusing optic of the instrument is changed, the easiest solution is the reduction of the spot size of the beam by means of a mask (diaphragm). In applying this solution, however, the following precautions must be taken:

- provide a mechanical system able to ensure the perfect repositioning of the mask each time it is removed, for example to place the sample after the baseline measurement
- arrange the mask **before** the sample along the beam path, for both transmittance and reflectance measurements
- in the case of hemispherical reflectance, in addition to performing the baseline and the measurement of the sample, the contribution of the mask must also be considered by performing a third scan without placing neither the sample nor the reference. This spectrum has to be subtracted from both the baseline and the sample spectrum, since the final value is given from by their ratio

### B.5 Irregular thickness of the thin film

Another feature that is often observed on thin film samples made in research laboratories is a marked non-uniformity of the thickness. The consequence is the imperfect correspondence between the positions of the maxima and minima of the interference fringes in the reflectance and transmittance spectra of thin film.

The solution is to mark the sample and arrange it in such a way that the spot of the measuring beam, having a typical banana shape, impinges on the same area of the sample for all measurements.

## B.6 Scan speed and integration time

Currently the most common UV-VIS-NIR spectrophotometers belong to the dispersive type. Unlike those belonging to the FTIR type (Fourier transform) commonly used for measurements in the IR region, in dispersion instruments the acquisition of the spectrum is obtained by changing the wavelength of the measure beam step by step; this implies a rather long acquisition time. So the neophyte, to hurry up the measurement, is inclined to select the highest speeds allowed by the software of the instrument (for example 480 nm/min), without evaluating the possible consequences: as a matter of fact in the case of spectra with sharp variations, such as the case of the transmittance UV cutoff of glass substrates or the interference fringes of thin film of sufficient thickness, the measured spectrum will be distorted both by the smoothing of maxima and minima (reduction of the peak-valley amplitude), and by the shift of the transients to UV, if scanning speed and instrument integration time are not well balanced. The latter artefact is caused by the reading delay combined with the scan direction of the selected range, from the maximum wavelength to the minimum one.

The presence of such artefacts can be verified by comparing the value of a static measurement reading (at a fixed wavelength), with the corresponding value in the spectrum, dynamically acquired. If the difference is greater than the measurement error, a better compromise between scanning speed and integration time has to be found.

Whenever a session of measures is undertaken on a different type of samples, careful analysis of this critical point is required.

## B.7 Jump at the grating-detector change

A sharp jump is frequently observed in the spectra obtained with dispersion instruments, at the wavelength at which grating and detector are changed (typically 860 nm). Normally this phenomenon is less marked if an integrating sphere is used.

To overcome this problem it is necessary to balance the width of the slits (kept to a constant value in the UV-VIS region) with the electronic gain of the sensor used in the NIR. Sometimes it can be useful to modify the change wavelength, so as to make the intensity of the measurement signal more similar on both sides.

## B.8 Misaligned spectrophotometer

A periodical check of the optical alignment of the spectrophotometer is strongly recommended. This operation requires a good experience of optical beam manipulation by the user. Otherwise a technical intervention is advisable or at least the supervision by a more experienced colleague.

The main check is to verify that the two beams (measure and reference) are well aligned both in and downstream of the sample holder compartment. Some software are equipped with tools for alignment diagnostics and sometimes self-optimizing hardware.

In my experience, the most serious and frequent episodes occur with integrating spheres, especially when they are frequently disassembled and reinstalled. In this case, by setting the instrument on white or green light, in dark-room conditions, the operator must verify that the beams pass in the centre of the entrance and exit ports. In case of imperfections, the return mirrors upstream to the sphere have to be adjusted.

## References

- [1] M. Montecchi, E. Nichelatti, and P. Polato, Hybrid equivalent model algorithm or the prediction of glazing angular properties, *Solar Energy Materials and Solar Cells* **71**, 327–342 (2002).
- [2] E. Nichelatti, M. Montecchi, and R. M. Montereali, Optical reflectance and transmittance of a multilayer coating affected by refractive-index inhomogeneity, interface roughness, and thickness wedge, *J. Non-Cryst. Solids* **355**, 1115–1118 (2009).
- [3] M. Montecchi, E. Masetti, and G. Emiliani, Thickness and model optimization in characterization of optical interference films by using discontinuities of  $n(\lambda)$  solutions, *Pure Appl. Opt.* **4**, 15–26 (1995).
- [4] M. Montecchi, Characterization of inhomogeneous optical interference films using a complex parabolic profile model, *Pure Appl. Opt.* **4**, 831–839 (1995).
- [5] D. Stroud, The effective medium approximations: some recent developments, *Superlattices and Microstructures* **23**, 567–573 (1998).
- [6] R. E. Denton, R. D. Campbell, and S. G. Tomlin, The determination of the optical constants of thin films from measurements of reflectance and transmittance at normal incidence, *J. Phys. D: Appl. Phys.* **5**, 852–863 (1972).
- [7] M. Montecchi, A. Mittiga, C. Malerba, and F. Menchini, KSEMAW: an open source software for the analysis of spectrophotometric, ellipsometric and photothermal deflection spectroscopy measurements [version 2; peer review: 2 approved], *Open Research Europe* **1**(95) (2023).
- [8] M. Born and E. Wolf, *Principles of Optics*, Pergamon Press, Oxford, 6th edition, 1987.
- [9] A. Yariv, *Quantum Electronics*, John Wiley & Sons, 2nd edition, 1989.
- [10] R. Boyd, *Nonlinear Optics*, Academic Press, 2nd edition, 2003.
- [11] K. Prokopidis and C. Kalialakis, Physical interpretation of a modified Lorentz dielectric function for metals based on the Lorentz - Dirac force, *Appl. Phys. B* **117**, 25 – 32 (2014).
- [12] L. Landau and E. Lifshitz, *The classical theory of fields*, Pergamon, Oxford, 1962.
- [13] P. Etchegoin, E. Le Ru, and M. Meyer, An analytic model for the optical properties of gold, *Journal of Chemical Physics* **125**, 164705 (2006).
- [14] K. Prokopidis and D. C. Zografopoulos, A Unified FDTD/PML Scheme Based on Critical Points for Accurate Studies of Plasmonic Structures, *Journal of lightwave Technology* **31**, 2467 – 2476 (2013).
- [15] A. Deinega and S. John, Effective optical response of silicon to sunlight in the finite-difference time-domain method, *Optics Letters* **37**, 112 – 114 (2012).

- [16] C. Moore, C. M. Adhikari, T. Das, L. Resch, and U. Ullrich, C.A. Jentschura, Temperature-dependent dielectric function of intrinsic silicon: Analytic models and atom-surface potentials, *Phys. Rev B* **106**, 045202 (2022).
- [17] J. Leng, J. Opsal, H. Chu, M. Senko, and D. Aspnes, Analytic representations of the dielectric functions of materials for device and structural modeling, *Thin Solid Films* **313-314**, 132 – 136 (1998).
- [18] M. Montecchi, E. Nichelatti, R. M. Montereali, M. Piccinini, and F. Somma, Increase of refractive index induced by absorbing centres, *Opt. Quantum. Electron.* **36**, 43–55 (2004).
- [19] I. Hamberg and C. G. a. Granqvist, Evaporated Sn-doped In<sub>2</sub>O<sub>3</sub> films:Basic optical properties and application to energy-efficient windows, *J. Appl. Phys* **60**, R123 (1986).
- [20] D. Greiner, N. Papathanasiou, A. Pflug, F. Ruske, and R. Klenk, Influence of damp heat on the optical and electrical properties of Al-doped zinc oxide, *Thin Solid Films* **517**, 2291 – 2294 (2009).
- [21] D. Mergel and Z. Qiao, Dielectric modelling of optical spectra of thin In<sub>2</sub>O<sub>3</sub> : Sn films, *J. Phys. D: Appl. Phys.* **35**, 794 – 801 (2002).
- [22] P. Yu and M. Cardona, *Fundamentals of Semiconductors*, Springer, Berlin, 2001.
- [23] S. Schaefer, S. Gao, P. Webster, R. Kosireddy, and S. Johnson, Absorption edge characteristics of GaAs,GaSb, InAs, and InSb, *J. Appl. Phys.* **127**, 165705 (2020).
- [24] J. Tauc, R. Grigorovici, and A. Vancu, Optical properties and electronic structure of amorphous germanium, *Phys. Stat. Sol.* **15**, 627 (1966).
- [25] G. Cody, B. Brooks, and B. Abeles, Optical absorption above the optical gap of amorphous silicon hydride, *Solar Energy Mater.* **8**, 231 – 240 (1982).
- [26] R. J. Elliott, Intensity of Optical Absorption by Excitons, *Physical Review* **108**, 1384–1389 (1957).
- [27] C. Tanguy, Optical dispersion by Wannier excitons, *Phys. Rev. Lett.* **75**, 4090–4093 (1995).
- [28] B. Velicky and J. Sak, Excitonic effects in the interband absorption of Semiconductors, *Phys.Stat.Sol.* **16**, 147–157 (1966).
- [29] R. J. Jelitto, The density of states of some simple excitations in solids, *J. Phys. Chem. Solids* **30**, 609–626 (1969).
- [30] T. Ogawa and T. Ogawa, An analytical model for the density of states, *Physics Letters* **48A**, 51–52 (1974).